MARTIN MARIETTA ENERGY SYSTEMS LIBRARIES
3 4456 0283874 9

ORNL/TM-10466

ornl

OAK RIDGE NATIONAL LABORATORY

MARTIN MARIETTA

Fiber-Reinforced Ceramic Tubular Composites

A. J. Caputo and R. A. Lowden
Oak Ridge National Laboratory

H. H. Moeller
Babcock & Wilcox

OAK RIDGE NATIONAL LABORATORY
CENTRAL RESEARCH LIBRARY
CIRCULATION SECTION
4500N ROOM 175
LIBRARY LOAN COPY
DO NOT TRANSFER TO ANOTHER PERSON
If you wish someone else to see this report, send in name with report and the Library will arrange a loan.

OPERATED BY
MARTIN MARIETTA ENERGY SYSTEMS, INC.
FOR THE UNITED STATES
DEPARTMENT OF ENERGY

Fossil Energy Program

Printed in the United States of America. Available from
National Technical Information Service
U.S. Department of Commerce
5285 Port Royal Road, Springfield, Virginia 22161
NTIS price codes—Printed Copy: A06 Microfiche A01

This report was prepared as an account of work sponsored by an agency of the United States Government. Neither the United States Government nor any agency thereof, nor any of their employees, makes any warranty, express or implied, or assumes any legal liability or responsibility for the accuracy, completeness, or usefulness of any information, apparatus, product, or process disclosed, or represents that its use would not infringe privately owned rights. Reference herein to any specific commercial product, process, or service by trade name, trademark, manufacturer, or otherwise, does not necessarily constitute or imply its endorsement, recommendation, or favoring by the United States Government or any agency thereof. The views and opinions of authors expressed herein do not necessarily state or reflect those of the United States Government or any agency thereof.

ORNL/TM-10466

Metals and Ceramics Division

FIBER-REINFORCED CERAMIC TUBULAR COMPOSITES

A. J. Caputo and R. A. Lowden
Oak Ridge National Laboratory

H. H. Moeller
Babcock & Wilcox

Date Published – November 1988

NOTICE: This document contains information of a preliminary nature. It is subject to revision or correction and therefore does not represent a final report.

Prepared for the
AR&TD Fossil Energy Materials Program
AA 15 10 10 0

Prepared by the
OAK RIDGE NATIONAL LABORATORY
Oak Ridge, Tennessee 37831
operated by
MARTIN MARIETTA ENERGY SYSTEMS, INC.
for the
U.S. DEPARTMENT OF ENERGY
under Contract No. DE-AC05-84OR21400

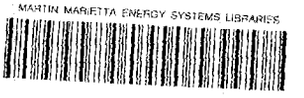

3 4456 0283874 9

CONTENTS

LIST OF FIGURES v
LIST OF TABLES vii
ABSTRACT 1
INTRODUCTION 1
EXPERIMENTAL PROCEDURE 2
    PREFORM FABRICATION 2
    INFILTRATION OF PREFORMS 3
    CHARACTERIZATION 10
        Matrix Distribution 10
        Density 11
        Relative Permeability 12
        Strength Testing 12
RESULTS 14
    INFILTRATION 18
    MATRIX DISTRIBUTION 21
    RELATIVE PERMEABILITY 25
    ROOM-TEMPERATURE TESTING 25
    ELEVATED-TEMPERATURE TESTING 30
DISCUSSION 32
CONCLUSIONS 37
ACKNOWLEDGMENT 37
REFERENCES 38

LIST OF FIGURES

Figure		Page
1	As-wound preforms. (*a*) Circumferentially wound, (*b*) angle wound (10° off hoop) with multiple-tow crossover, (*c*) angle wound (10° off hoop) with adjacent tows and aligned-tow crossover	4
2	Chemical vapor deposition system for infiltration of ceramic fiber preforms	6
3	Stainless-steel water-cooled injector	7
4	(*a*) Graphite gas distributor, (*b*) mandrel	8
5	Composite tube with section removed. (C-rings were cut from this tube for strength measurements)	11
6	Relative permeability of infiltrated composite determined with simplified gas-flow apparatus	13
7	Computerized mechanical testing system	15
8	Infiltrated tube – circumferentially (hoop) wound	19
9	Infiltrated tube – angle wound with adjacent tows and aligned-tow crossover	20
10	Matrix was distributed rather uniformly along tube length	22
11	Typical section of infiltrated silicon carbide fiber-reinforced silicon carbide	23
12	Pyrolytic carbon coating deposited on SiC fibers before deposition of SiC matrix. (*a*) Middle of tube, OD surface; (*b*) middle of tube, ID surface	24
13	Relative permeability of infiltrated tubes varied with tube density	26
14	Stress-strain curve of a specimen fractured at room temperature	27
15	Fractured C-ring tested at room temperature shows fiber pullout	28
16	Fracture surface of a specimen tested at room temperature shows fiber pullout	28

Figure		Page
17	Fiber-matrix interface of carbon-coated fiber composite following room-temperature tests	29
18	Stress-strain curve of a 90%-dense specimen tested at room temperature	30
19	Fracture surface of a 90%-dense specimen tested at room temperature	31
20	Fracture surface of a specimen tested at 1000°C in air shows fiber pullout	31
21	Fiber-matrix interface of carbon-coated fiber composite tested at 1000°C. (*a*) Area showing fibers with carbon coating, (*b*) area showing fibers with no carbon coating, (*c*) area showing fibers partly coated with carbon	33
22	Stress-strain curve of a 90%-dense specimen tested at 1000°C in air	34
23	Stress-strain curve of a 90%-dense specimen tested at 1200°C in air	34

LIST OF TABLES

Table		Page
1	ORNL-B&W tubular composites	9
2	Properties of infiltrated tubes	16
3	C-Ring strength of tubular composites	17

FIBER-REINFORCED CERAMIC TUBULAR COMPOSITES*

A. J. Caputo, R. A. Lowden, and H. H. Moeller†

ABSTRACT

Ceramic fiber-ceramic matrix tubular composites have been developed in a joint program of Oak Ridge National Laboratory (ORNL) and the Babcock & Wilcox Company. This program was the first collaborative agreement between a private industry and ORNL. The ceramic tubular composites were fabricated using a novel chemical vapor infiltration process developed at ORNL. Silicon carbide filament-wound preforms were infiltrated with additional silicon carbide to form the matrix phase of the composite. The tubular composites exhibited exceptional strength and strain tolerances that were significantly higher than monolithic (nonreinforced) SiC. C-ring strengths and fracture surface evaluation of both room-temperature- and elevated-temperature-tested specimens are presented.

INTRODUCTION

Ceramic fiber-ceramic matrix composites are receiving increased interest in the materials development community because of their potential high strength and toughness, especially at elevated temperatures. Nonreinforced (monolithic) ceramics have excellent high-temperature properties but suffer from brittle behavior. With continuing development, ceramic fiber-reinforced composites should be candidate materials for use in turbine and automobile engine components, heat exchangers, recuperators, and other high-temperature applications.

*Research sponsored by the U.S. Department of Energy, AR&TD Fossil Energy Materials Program [DOE/FE AA 15 10 10 0, Work Breakdown Structure Element ORNL-2(A)] under contract DE-AC05-84OR21400 with Martin Marietta Energy Systems, Inc.

†Babcock & Wilcox, Lynchburg, VA.

The preparation of composites using various fibers and matrices has been extensively reported.[1-7] The use of chemical vapor infiltration (CVI) processes to form the matrix of a fiber-reinforced composite also has been reported.[8-14] Before this joint effort with Babcock & Wilcox Company (B&W), the CVI process was being investigated at Oak Ridge National Laboratory (ORNL) as a means of fabricating ceramic fiber-reinforced composites in the shape of various size disks by infiltrating compressed multiple layers of woven Nicalon* (SiC) cloth.[15-20] During this work, a novel CVI process that combines thermal-gradient and forced-flow approaches was developed. The technique results in significantly reduced infiltration times compared with other systems that depend only on diffusion for entry of coating gases and exit of gaseous products.

The potential uses for ceramic composites (engine components, heat exchangers, recuperators, etc.) indicated a need for a means of producing cylindrical shapes. Additionally, to find broad commercial applications for this composite material, the technology needed to be transferred to the industrial community; thus, a joint program was established between ORNL and B&W to collaborate in the infiltration of tubular shapes that would exhibit improved mechanical properties. B&W, with expertise in forming fibrous tubes, prepared the filament-wound preforms at their Lynchburg, Virginia, facility. The wound preforms were infiltrated at ORNL by using the novel infiltration process adapted for the tubular shape. The infiltrated composites were evaluated at ORNL for the effect of process conditions on uniformity of infiltration. C-ring strength testing at both room and elevated temperature and evaluation of the resulting fracture surfaces were done at B&W.

EXPERIMENTAL PROCEDURE

PREFORM FABRICATION

Cylindrical preforms were prepared by filament winding and had an ~51-mm (2-in.) OD, a nominal 127-mm (5-in.) length, and 6-mm (0.25-in.)

*Nippon Carbon Co., Tokyo, Japan.

wall thickness. The tubes were wound using a continuous tow of Nicalon fibers that contained ~500 fibers per tow with individual fibers having a diameter of 10 to 15 μm. Although Nippon Carbon markets a standard and a ceramic grade of Nicalon fibers, only the ceramic grade was used in this program.

All preforms were unidirectionally wound, initially in the hoop direction [Fig. 1(*a*)]. A single spool was used to feed an automatic fiber-winding apparatus. Teflon spools were used at first to guide the Nicalon tows, but after difficulty with the teflon thread guides was experienced, porcelain thread guides were substituted. The density of the fiber preform was adjusted by controlling the tension on the fiber feed spool. Near the end of the program, several preforms were fabricated with the fiber direction 10° off the hoop direction to provide strength in both the axial and radial directions. Two feed spools were used to fabricate these specimens.

In addition to the fiber preforms fabricated at B&W, the Oak Ridge Gaseous Diffusion Plant (ORGDP) fabricated two unidirectionally wound preforms. The first preform was similar to the later B&W preforms with the fiber wound 10° off the hoop direction. However, the winding technique resulted in space between the tows and a multiple crossover pattern of the tows [Fig. 1(*b*)], producing some alignment of large pores and, thus, large flaws that adversely affected the strength of the infiltrated tube. The second tube was prepared using a different fiber-winding apparatus that made it possible to wind a preform not only with adjacent tows essentially touching each other, but also with the crossover points aligned at regular intervals along the axis of the tube [Fig. 1(*c*)]. This winding prevented the formation of large pores.

INFILTRATION OF PREFORMS

The matrix phase of the composites was formed by a CVI process developed at ORNL that combines a thermal gradient and pressure gradient to greatly reduce infiltration time.[21] The first major goal of this effort was to adapt the ORNL infiltration system for use with the tubular configuration. To accomplish this, the key items of the process, the water-cooled gas distribution system and the fibrous preform, were designed and fabricated. Two versions of the gas distribution systems were designed,

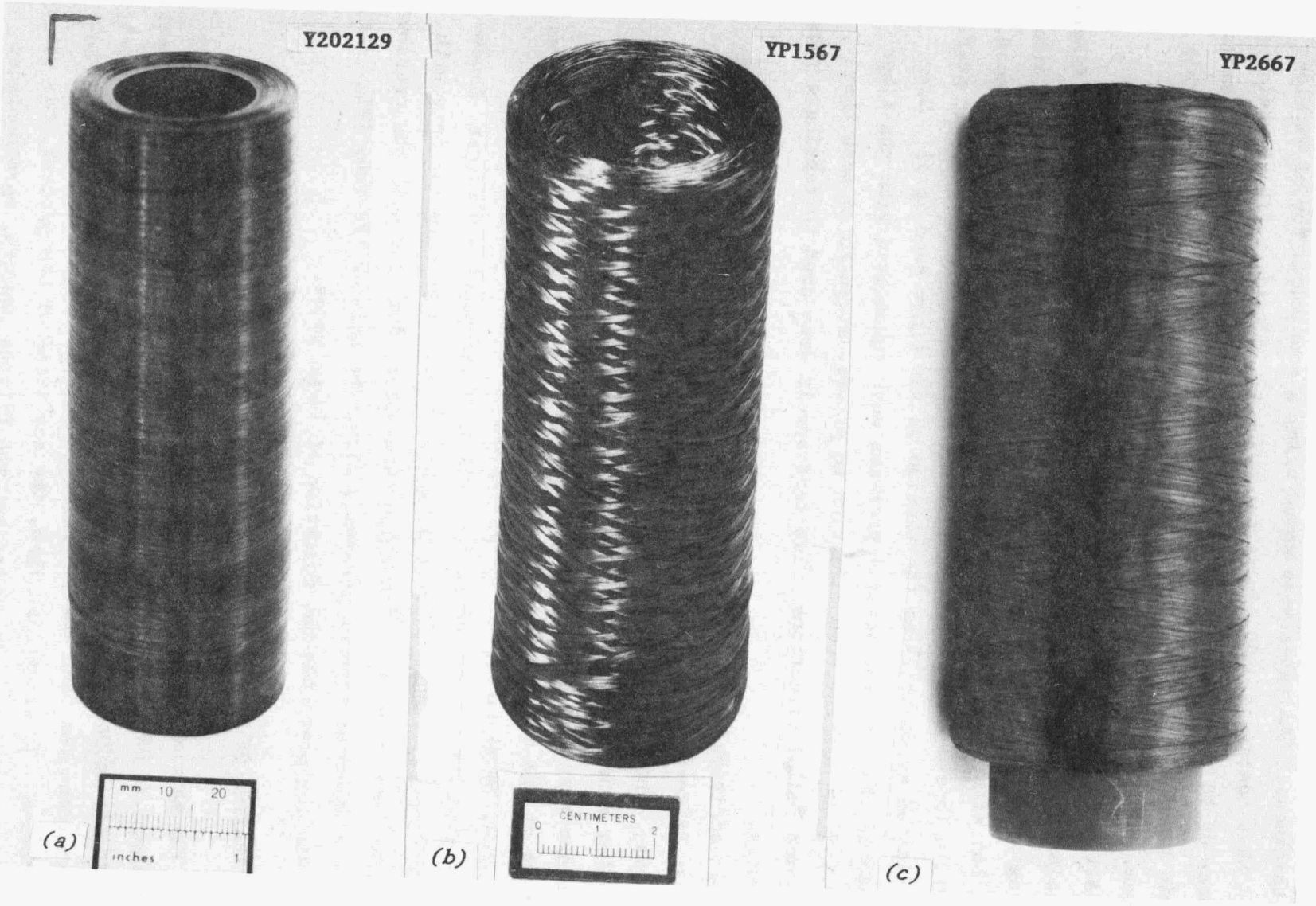

Fig. 1. As-wound preforms. (*a*) Circumferentially wound, (*b*) angle wound (10° off hoop) with multiple-tow crossover, (*c*) angle wound (10° off hoop) with adjacent tows and aligned-tow crossover.

one introducing the gases near the base (bottom) of the preform, and the other with the gases entering near the top of the preform. After initial testing the first model was chosen and a schematic of the system is shown in Fig. 2. The water-cooled injector (Fig. 3) provided reactant gas-flow passage into the infiltration furnace and the cooling-water flow required to keep the metal injector cool. The cooled injector, in turn, cooled the graphite gas distributor, which cooled both the inside diameter and base surfaces of the preform. A Si_3N_4-BN thermal insulator at the bottom of the preform aided in the control of the amount of cooling. Thus, the incoming reactant gases passed through the cooled inner surfaces of the preform without reacting. Deposition occurred as the reactant gases approached the higher-temperature regions near the outer surfaces of the preform. The ability to maintain relatively high gas flows, to control deposition in the higher-temperature region of the part, and to avoid early deposition at the inlet surfaces (which would blind the surfaces and terminate the infiltration) resulted in much higher deposition rates than those obtained with other processes.

Hydrogen and methyltrichlorosilane (MTS) reactant gases were distributed by the multiple slots of the graphite gas distributor and the multiple holes of the graphite mandrel (Fig. 4). Deposition of the SiC matrix continued until most of the porosity of the preform was filled and the resistance to the flow of the reactant gases increased to a back pressure of 170 kPa abs. The infiltration process occurred in a 1473 K furnace (as measured optically on the top cover of the tube), using flows [standard temperature and pressure (STP)] of 75-cm^3/min MTS and 750-cm^3/min hydrogen, except as noted in Table 1.

During the early phase of the project, the deposition temperature was periodically determined during a run with an optical pyrometer, and power adjustments were made manually. An automated system was installed during the later stages of the program to provide continuous control of the temperature. A single-color pyrometer* continuously monitored the temperature, and control circuitry made the necessary power adjustments.

---

*IRCON, Inc., Modline 2000, Niles, IL.

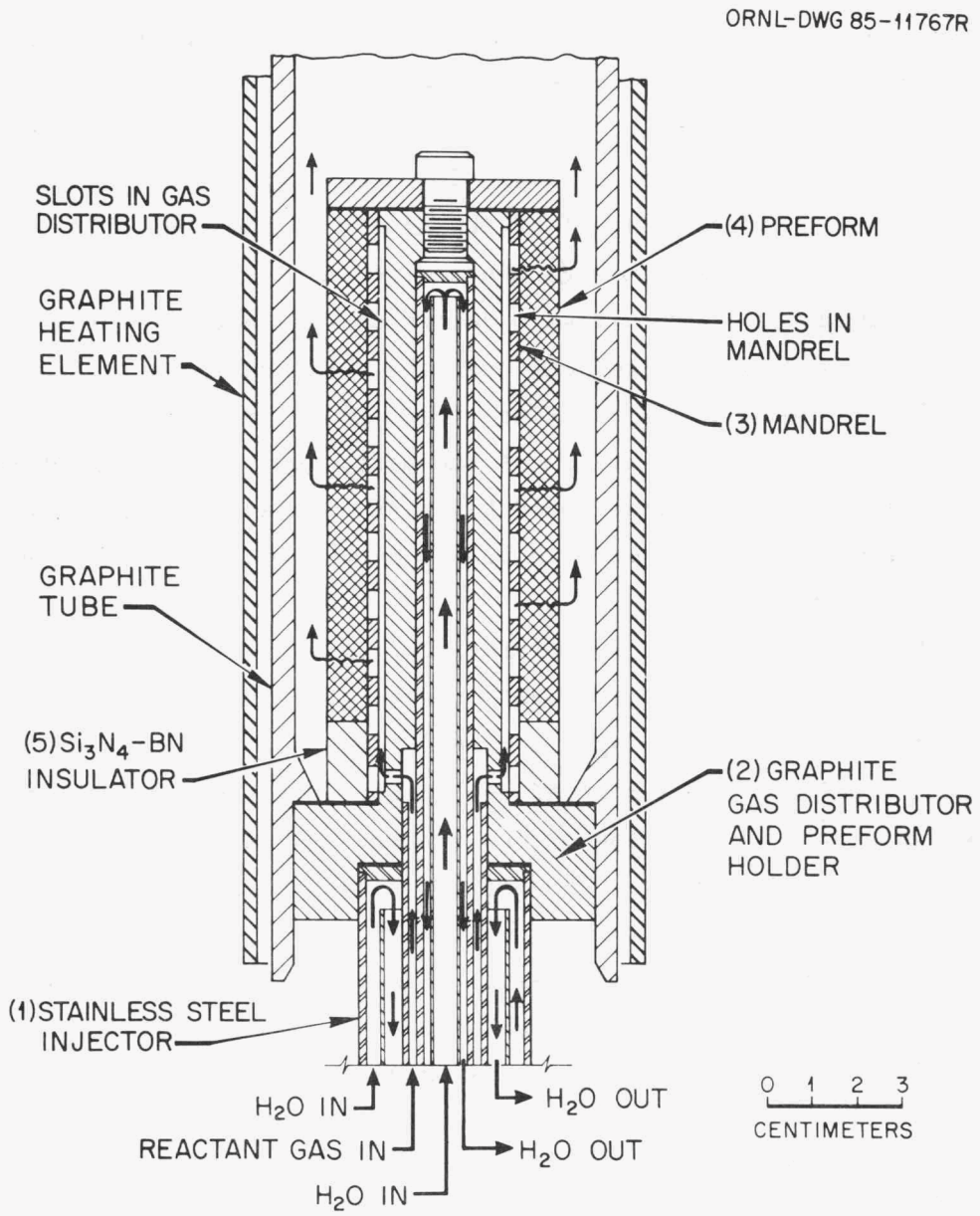

Fig. 2. Chemical vapor deposition system for infiltration of ceramic fiber preforms.

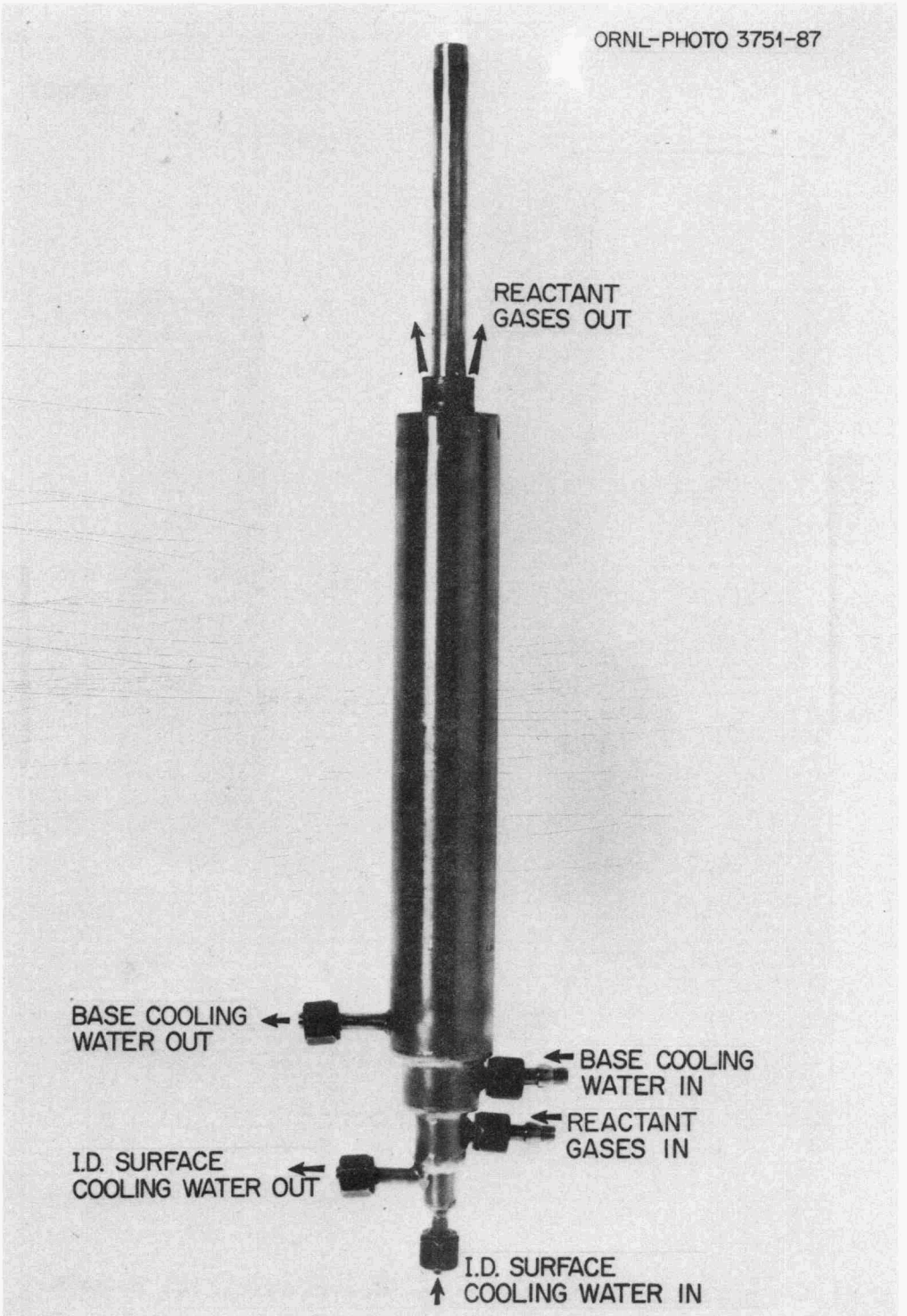

Fig. 3. Stainless-steel water-cooled injection.

YP3885

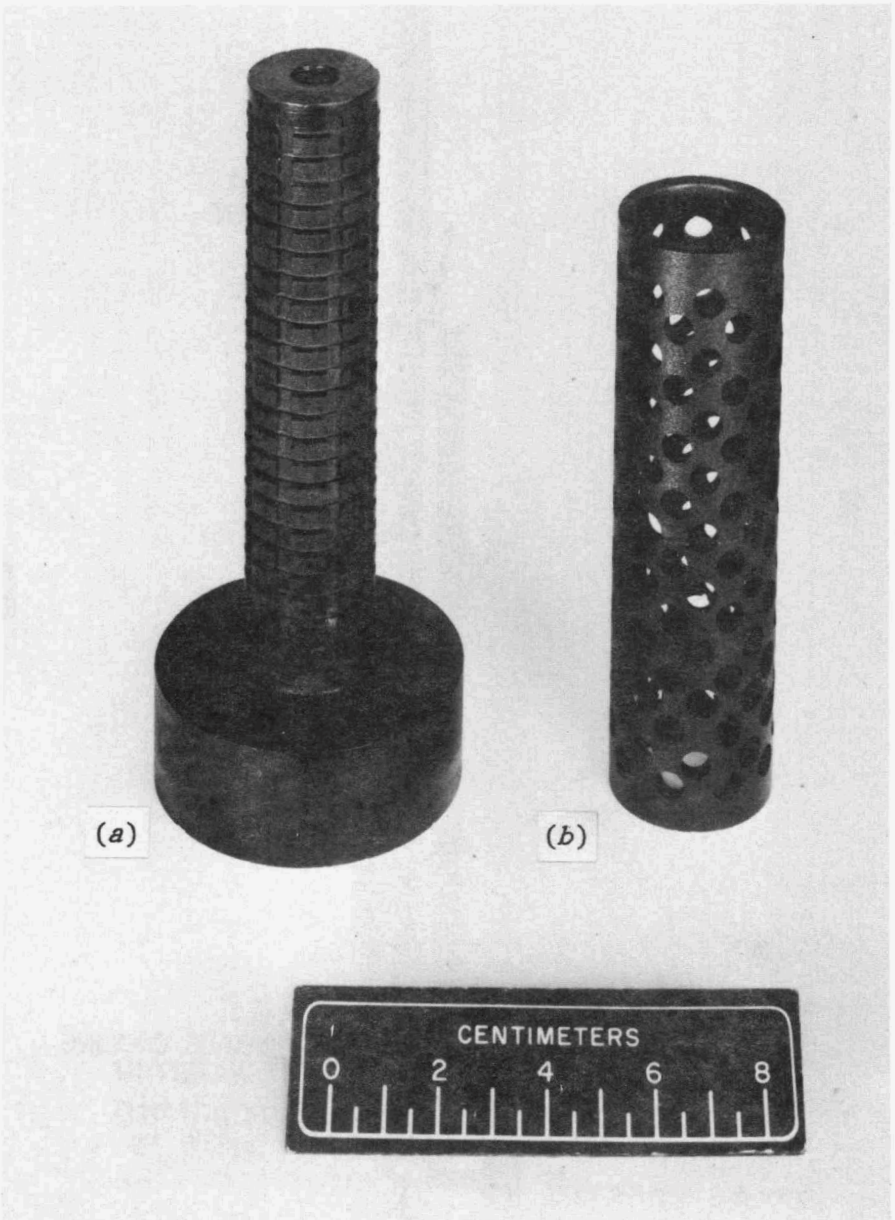

Fig. 4. (*a*) Graphite gas distributor, (*b*) mandrel.

Table 1. ORNL-B&W tubular composites

Run No. (BW)	Preform characteristics			Infiltration conditions		
					Gas flows	
	Type winding	Size, OD × ID × length (cm)	Fiber content (vol. %)	Temp. (K)	MTS (cm^3/min)	Hydrogen (cm^3/min)
19	Angle	5.1 × 3.8 × 12.3	47.4	1473	75	750
18	Angle	5.1 × 3.8 × 11.1	41.2	1473	75	750
17	Angle	5.1 × 3.8 × 11.1	43.1	1473	75	750
16	Circumferential	5.1 × 3.8 × 11.4	53.7	1473	75	750
15	Angle	5.1 × 3.8 × 11.0	37.3	1473	75	750
14	Angle	4.8 × 3.8 × 10.6	41.8	1473	75	750
13	Angle	4.8 × 3.8 × 12.7	48.0	1473	75	750
12	Circumferential	5.1 × 3.8 × 12.7	49.6	1473	75	750
11	Circumferential	4.8 × 3.8 × 12.4	45.7	1473	50	500
10	Circumferential	5.1 × 4.1 × 13.0	54.7	1473	100	1000
9	Circumferential	5.1 × 3.8 × 13.0	41.7	1473	150	1500
8	Circumferential	5.1 × 3.8 × 13.0	50.8	1473	150	1500
7	Circumferential	5.1 × 3.8 × 13.0	48.5	1473	150	1500
6	Circumferential	4.6 × 3.6 × 13.1	55.0	1473	50-150	500-1500
5	Circumferential	5.1 × 3.8 × 13.0	41.5	1473	150	1500
4	Circumferential	4.3 × 3.0 × 12.1	37.5	1473	50	500
3	Circumferential	4.6 × 3.3 × 13.0	36.3	1473	50	500
2[a]	Circumferential	3.8 × 2.5 × 2.5	~30	1473	50	500
1	Circumferential	3.8 × 2.5 × 2.5	30.2	1473	50	500

[a]Incomplete infiltration.

Initially, the flow of MTS was controlled by the flow of the hydrogen carrier (rotameter controlled) through the MTS evaporator at a given temperature. The average MTS flow for a run was determined by the weight loss of the evaporator but could not be continuously indicated or controlled during the run. Later in the program, continuous control was obtained with the installation of an automated flow system using mass flow meters and flow controllers. The predetermined total hydrogen flow was controlled by a mass flow controller* with a portion of this flow being diverted through the MTS evaporator. The actual flow of MTS was continuously monitored by another mass flow controller† that varied the amount of hydrogen flow diverted through the evaporator to maintain a constant MTS flow. In this manner, the system maintained a constant MTS flow, a constant total hydrogen flow, and, consequently, a constant ratio between the two.

In several of the later runs, the fibers in the preform were precoated with a thin layer of carbon to protect the fibers and to weaken the bond between the fibers and the matrix. Compared with the brittle fracture normally associated with nonreinforced ceramics, the carbon layer enhanced the desired fiber pullout and promoted nonbrittle fracture. The carbon was deposited using flows (STP) of 100 cm^3/min of propylene and 500 cm^3/min of argon at 1373 K at ~13 kPa (~100 torr) for periods ranging from 4 to 7 h.

CHARACTERIZATION

Matrix Distribution

An axial section was removed from the infiltrated tube by cutting with a diamond saw, which left the remaining tube in the C-ring configuration (Fig. 5) required for strength testing. The removed section was cut into three pieces, representing the top, middle, and bottom portions of the infiltrated tube. Each piece was vacuum-mounted in epoxy, cut in half axially, and the cut surfaces ground and polished for optical viewing.

The polished surfaces were examined at low magnification (5×) to assess the overall uniformity of the wound fibers and the infiltrated

---

*MKS Instruments, Inc., Type 1259A, Burlington, MA.

†Tylan, Source V, Carson, CA.

YP6308

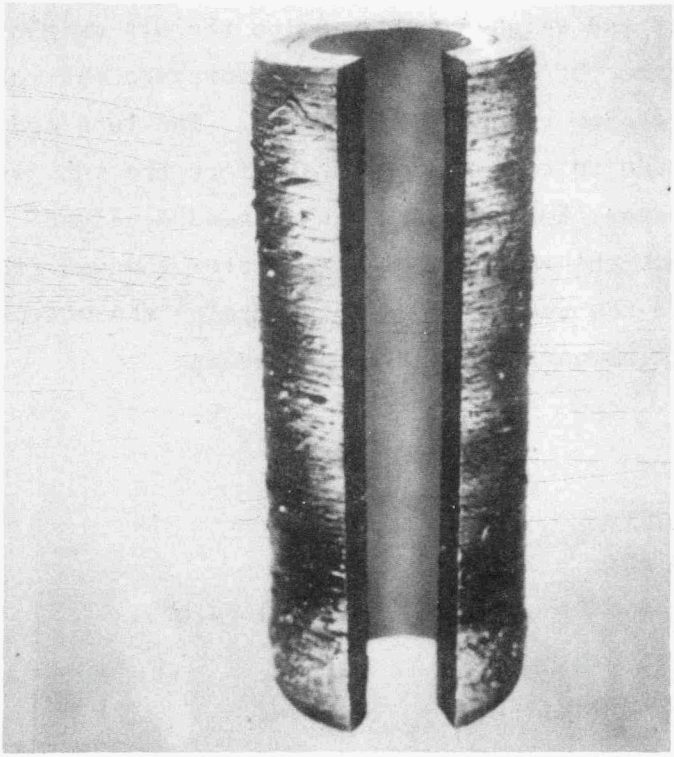

Fig. 5. Composite tube with section removed. (C-rings were cut from this tube for strength measurements.)

matrix and at higher magnification (200 to 500×) to reveal details and to examine the fiber-matrix interface. When the fibers were precoated with pyrolytic carbon, oil-immersion viewing at 3000× with polarized light revealed both the distribution and thickness of the pyrolytic carbon.

Density

Two methods, geometrical and immersion, were used to determine density. Geometrical density was used to describe the fiber loading in the preform and the properties of the C-rings. The immersion-density method was used to determine more accurately the density of the entire infiltrated tube.

The geometrical density was determined from the weight and the calculated volume of the tube. The values used for the outside diameter and the length of the tube in the volume calculation were averages of three individual measurements. The value used for the inside diameter was the outside diameter of the machined mandrel.

To determine the immersion density, the tube was first dried in air at 343 K overnight and weighed to determine the dry weight. The tube was then placed in a beaker of water, and the temperature was increased to boiling for 1 h to eliminate trapped air bubbles. The tube and water were then allowed to return to room temperature before the tube was weighed (while suspended in water) to determine the suspended weight. Finally, the tube was removed from the water, the excess water removed from the surface with wet towels, and the tube weighed to determine the wet weight. The density B_1 was then determined from the relationship

$$B_1 = D/V \quad ,$$

where

D = dry weight,

V = volume = W−S/density of water (1 g/cm^3),

W = wet weight,

S = suspended weight.

Relative Permeability

Following infiltration, an estimate of the completeness of infiltration was made by determining the resistance to gas flow through the tube wall. Using the apparatus shown in Fig. 6, argon was introduced into the center of the tube and forced to flow through the tube wall. The argon flow rate required to maintain a given pressure inside the tube was used as a measure of relative permeability. The tests were performed at room temperature and atmospheric pressure.

Strength Testing

Mechanical strength of the composite was determined using a C-ring diametral compression test.[22-23] An advantage of this technique (in addition to ease of specimen machining) is that fracture is initiated along the outside surface of the C-ring where the tensile stresses are highest. The C-ring test also has been used at ORNL as a means of evaluating tubular specimens exposed to coal ash.[24-25] The fracture stress σ was calculated from the expression

$$\sigma = \left(\frac{P}{(r_o - r_i)w}\right)\left(1 + \frac{r_o + r_i}{2\,r_o}\right)\left(\frac{R - r_o}{r - R}\right) ,$$

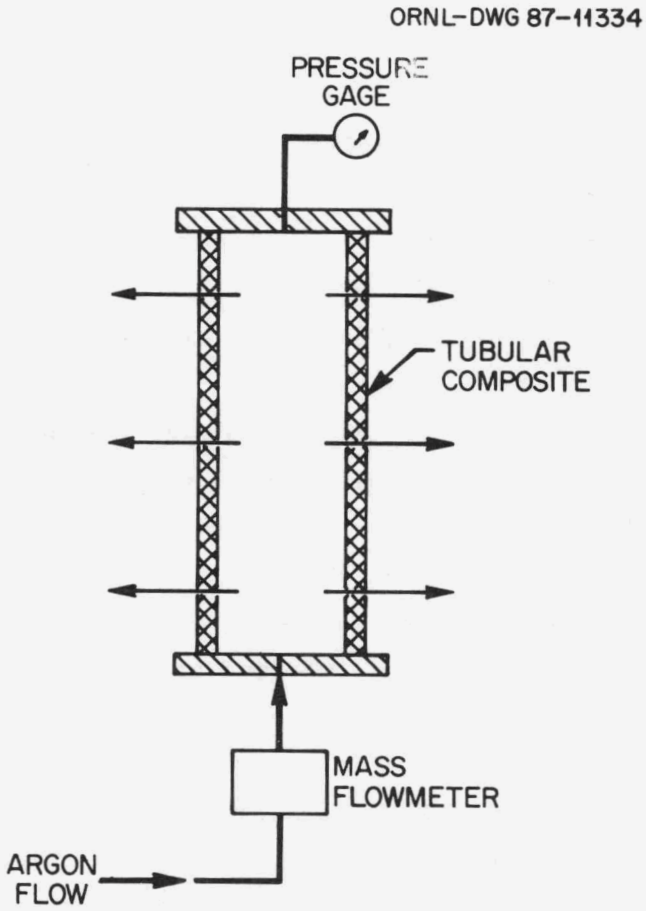

Fig. 6. Relative permeability of infiltrated composites determined with simplified gas-flow apparatus.

where

P = breaking load (negative for compressive loading),

r_o = OD/2 = outer radius,

r_i = ID/2 = inner radius,

$\bar{r} = (r_o + r_i)/2$,

R = radius of neutral axis = $(r_o - r_i)/\ln (r_o/r_i)$,

w = specimen width.

The equation used to calculate the strain was derived by T. S. Brown of B&W:[26-27]

$$\text{Strain} = \left(\frac{2\Delta}{\pi \bar{r} w t + Fo}\right) \left(\frac{6R}{t} - 1\right),$$

$$\text{where } Fo = \frac{12\bar{r}^2}{wt^3} + \frac{1}{wt} + \frac{E/G}{wt} ,$$

$\bar{r}$ = average radius of specimen,

w = specimen width,

t = specimen thickness,

Δ = deflection or displacement,

E/G = ratio of Young's modulus to the shear modulus.

The terms 1/wt + (E/G)/wt represent the membrane and shear deformation in a C-ring. These values are normally small compared with the bending deformation represented by $12\bar{r}^2/wt^3$. Therefore, in this study, the membrane and shear deformation contribution to the strain was neglected.

C-ring testing was conducted using a computer-controlled MTS* testing machine (Fig. 7). Tests were performed at room temperature, 1273 K, and 1473 K in air. For elevated-temperature testing, a furnace with a temperature capability of 1873 K in air was used.

In preparation for C-ring strength testing, C-ring specimens that had a nominal outside diameter of 51 mm (2 in.) and thickness of 6.4 mm (0.15 in.) were cut from the tube. All specimens were dried overnight in an oven set at 373 K. For elevated-temperature testing, specimens were soaked for 1 h at test temperature to ensure uniform temperature distribution in the test specimen.

Each specimen was preloaded to 1.0 kg (2.2 lb) and tested in compression at a displacement rate of 0.51 mm/min (0.02 in./min). After testing, the specimens were removed and examined visually and with scanning electron microscopy.

RESULTS

This was a development program in which 19 tubular specimens were fabricated (Tables 1, 2, and 3). Early in the program (run no. 3), one hoop-wound preform was infiltrated and resulted in a tubular specimen

---

*MTS Systems Corp., Minneapolis, MN.

YP6311

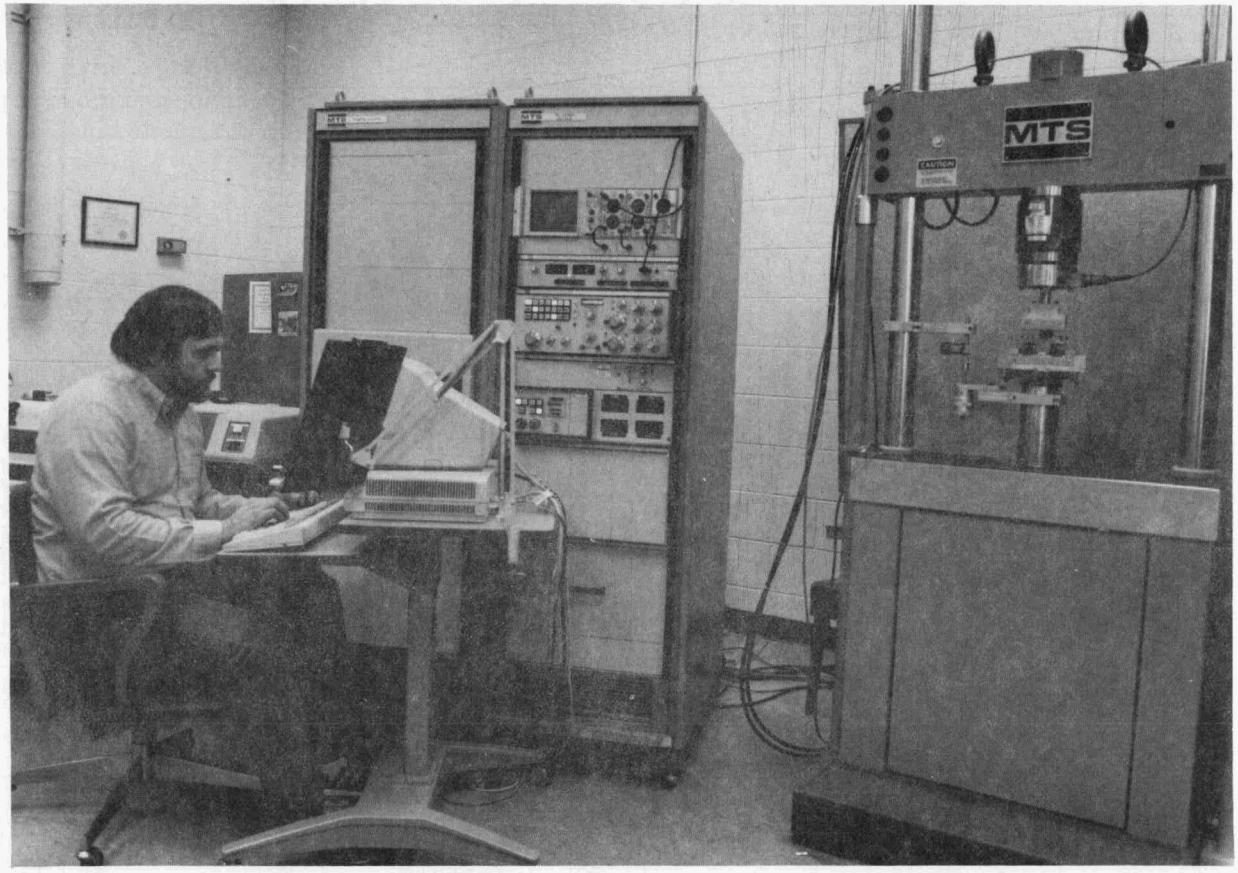

Fig. 7. Computerized mechanical testing system.

Table 2. Properties of infiltrated tubes

Run No.	Time (h)	No. of infiltrations	Weight gain (g)	Density[a] (g/cm^3)	% of theor. density[b]	Carbon interlayer thickness (μm)		Relative[c] permeability (L/min)	
						OD	ID	(34.5 kPa)	(69 kPa)
19	53.0	6	181	2.60	89.7			1.54	3.07
18	47.0	6	135	2.29	81.2	0.5-2.6	0.2-1.0	2.04	4.25
17	37.0	5	93	2.25	81.7	0.4-3.2	0.2-3.5	1.91	4.15
16	33.0	6	72	1.89	68.5	~0.5-2.5	~0.2-1.0		
15	47.5	8	189	2.47	83.4				
14	24.5	4	105	2.37	80.9				
13	47.5	8	125	2.32	80.2				
12	65.0	8	142	2.30	80.0				
11	70.0	10	94	2.16	74.3				
10	37.0	5	90	2.10	73.7				
9	42.0	6	161	2.46	83.9				
8	23.0	3	118	2.30	80.0				
7	11.0	3	73	1.87	64.6				
6	33.0	5	72	1.98	69.3				
5	38.0	6	135	2.44	83.0				
4	7.0	1	18	1.19	40.2				
3	62.0	11	117	2.13	71.8				
2	19.0	3	16						
1	22.0	4	25	2.24	74.4				

[a]For runs 1 through 9 density obtained from dimensional measurements; for runs 10 through 19 density obtained from immersion technique.

[b]Theoretical density is defined as the sum of the products of volume fraction and reported density of the components of the composite (fibers, precoat, and matrix).

[c]Argon flow at pressure differential of 34.5 or 69 kPa (5 or 10 psi) across tube wall.

Table 3. C-Ring strength of tubular composites

Run No.	Room temperature (air)					1273 K (air)					Comments
	Location	Strength (ksi)	Strength (MPa)	% of theor. density	Composite behavior	Location	Strength (ksi)	Strength (MPa)	% of theor. density	Composite behavior	
19	Top	87.9	606	77.8	No	Top	35.2	243	79.4	Yes	Repeat of #13; no PyC; reversed tube during run; used Si_3N_4-BN insulator; *tested at 1473 K in air.
	Bottom	88.5	610	73.6	No	Bottom	15.0	103	71.3	Yes	
						Top	24.5	169		Yes*	
18	Top	80.7	557	71.9	Partial	Top	51.5	355	71.7	Yes	Special winding at ORGDP; PyC thickness: OD = 0.5–2.6 μm, ID = 0.2–1.0 μm; started using automatic temperature controller on this run; used Si_3N_4-BN insulator.
	Middle	79.4	548	69.3							
	Bottom	117.5	810	70.7		Bottom	71.1	490	71.0	Yes	
17	Top	55.7	384	63.8	Yes	Top	11.7	81		Yes	PyC thickness; OD = 0.4–3.2 μm; ID = 0.2–3.5 μm; started using automatic MTS flow controller on this run; used Si_3N_4-BN insulator.
	Middle	66.5	459	69.0							
	Bottom	97.7	674	72.0	Partial	Bottom	44.3	306		Yes	
16	Top	14.1	97	62.1	No						Circumferential-wound tube to get data on axial strength; fibers precoated with pyrolytic carbon; used Si_3N_4-BN insulator.
	Bottom	30.0	207	64.2	Yes						
15	Top	62.2	428	74.3	No						ORGDP angle-wound preform with multiple tow crossover points; used Si_3N_4-BN insulator.
	Bottom	86.9	599	84.5	No						
14	Top	100.9	696	81.3	No	Top	60.2	415	82.8	Partial	Started using Si_3N_4-BN insulator.
	Bottom	65.3	450	80.3	No	Bottom	41.8	288	80.4	Yes	
13	Top	96.4	665	81.9	Yes	Top	26.4	182	72.9	Yes	First angle-wound preform with multiple tow crossover points; reversed tube position during run.
	Middle	88.9	280	80.2	No						
	Bottom	40.6	613	83.0	Yes						
12	Top	15.2	105	73.7	Yes						Multiple-hole graphite mandrel; multiple-slot graphite distributor; increased flows to 1.5× normal.
	Middle	59.2	408	79.6	No						
	Bottom	59.4	410	82.2	Partial						
11	Top	25.8	178	72.8	Yes						Used a graphocell mandrel; Nicalon fibers overcoated with BN by vendor[a] but could not be detected in infiltrated tube.
	Middle	25.6	177	70.2	Partial						
	Bottom	32.0	221	68.6	Yes						
10	Top	19.3	133	67.5							Used a graphocell mandrel; used 2x flows.
	Middle	24.1	166	73.3							
	Bottom	30.4	210	69.5							
9	Top	24.1	166	72.5	Yes						Used 3× flows; self-supporting preform (no mandrel); used 10.2-cm-high (4-in.) gas deflector; matrix deposition not uniform.
	Middle	54.7	377	75.7	No						
8	Top	24.9	172	68.3	Yes						Used 3× flows; self-supporting preform (no mandrel); used 5.1-cm-high (2-in.) gas deflector; thick coating on OD surface.
	Bottom	9.6	66	71.4	No						
7	Top	26.3	181	65.0	Yes						Used 3× flows; self-supporting preform (no mandrel); matrix deposition not uniform (thick coating on ID surface).
	Bottom	7.8	54	57.0	Yes						
6	Top	40.7	281	62.0	Yes	Top	7.2	50	71.5	Yes	Flows varied from 1× to 3×; 1% of fibers were Silar whiskers; used graphite mandrel and gas distributor with slots.
	Middle	56.9	392	65.0	Yes	Middle	22.0	152	65.0	Yes	
	Bottom	31.0	214	60.0	No						
5	Top	50.7	350	75.0	Yes	Top	12.5	86	80.0	Yes	Increased flows to 3×; used graphite mandrel and gas distributor with slots.
	Middle	56.4	389	78.0	No						
	Bottom	49.4	341	74.0	Yes						
4											Used injector type 2: run not completed; tube not tested.
3	Top	31.9	220	74.0	Yes	Top	6.2	43	63.0	Yes	First infiltration of 12.7-cm-long (5-in.) tube; injector type 1; used graphite mandrel with a few holes.
	Middle	76.6	528	75.0		Middle	40.5	279	73.0	Yes	
	Bottom	64.6	446	72.0	Yes	Bottom	20.8	143	61.0	Yes	
2											Used modified disk setup; incomplete densification.
1	Top	49.6	342		Yes						Used modified disk setup.
	Middle	22.7	157		No						
	Bottom	31.9	220		No						

[a]Synterials Inc., Herndon, VA.

with a C-ring strength of 528 MPa (76 ksi) at room temperature and 279 MPa (40 ksi) at 1273 K in air. At both temperatures, good composite behavior (strength retention following attainment of a maximum strength load) was observed.

In the remaining runs, several parameters were changed to establish conditions required for greater density, strength, and toughness and for simplified processing. The fiber loading of the preforms varied from 23 to 56% of theoretical, and the fiber angle was 10° off the hoop direction. The density of the composite tubes was typically in the range of 65 to 85% of theoretical (Table 2), and the strengths varied from 20 to 690 MPa (3 to 100 ksi) (Table 3). The ability of tubes to exhibit composite behavior during failure also varied during this period (Table 3). Generally, composites with 15 to 20% porosity exhibited excellent mechanical strength and composite behavior during failure. Near the conclusion of the program, several tubes were fabricated using the optimized parameters for both preforms and infiltration.

In an attempt to obtain more-consistent strength and composite-type behavior, the fibers of three of the last four preforms were coated with pyrolytic carbon before deposition of the SiC matrix. As a result, tubular specimens that had both good strength and good composite behavior were fabricated.

In the results, emphasis is placed on the hoop-wound tubes fabricated at the beginning of the program and the final 4 of the 19 tubes fabricated. These had densities ranging from 70 to 85% of theoretical; the last tube fabricated had an average density of 90% of theoretical.

Figures 8 and 9 show two of the finished tubes fabricated in this program that have a nominal dimension of 51-mm (2-in.) OD × 127 mm (5 in.) long. The tube shown in Fig. 8 was fabricated from a preform that was wound in the hoop direction; the tube shown in Fig. 9 was fabricated from a preform with the fiber direction 10° off the hoop direction.

INFILTRATION

The design of the gas distributor and preform mandrel are critical to the process because these two items transfer the cooling from the injector to the preform and uniformly distribute the reactant gas flows across the

YP6309

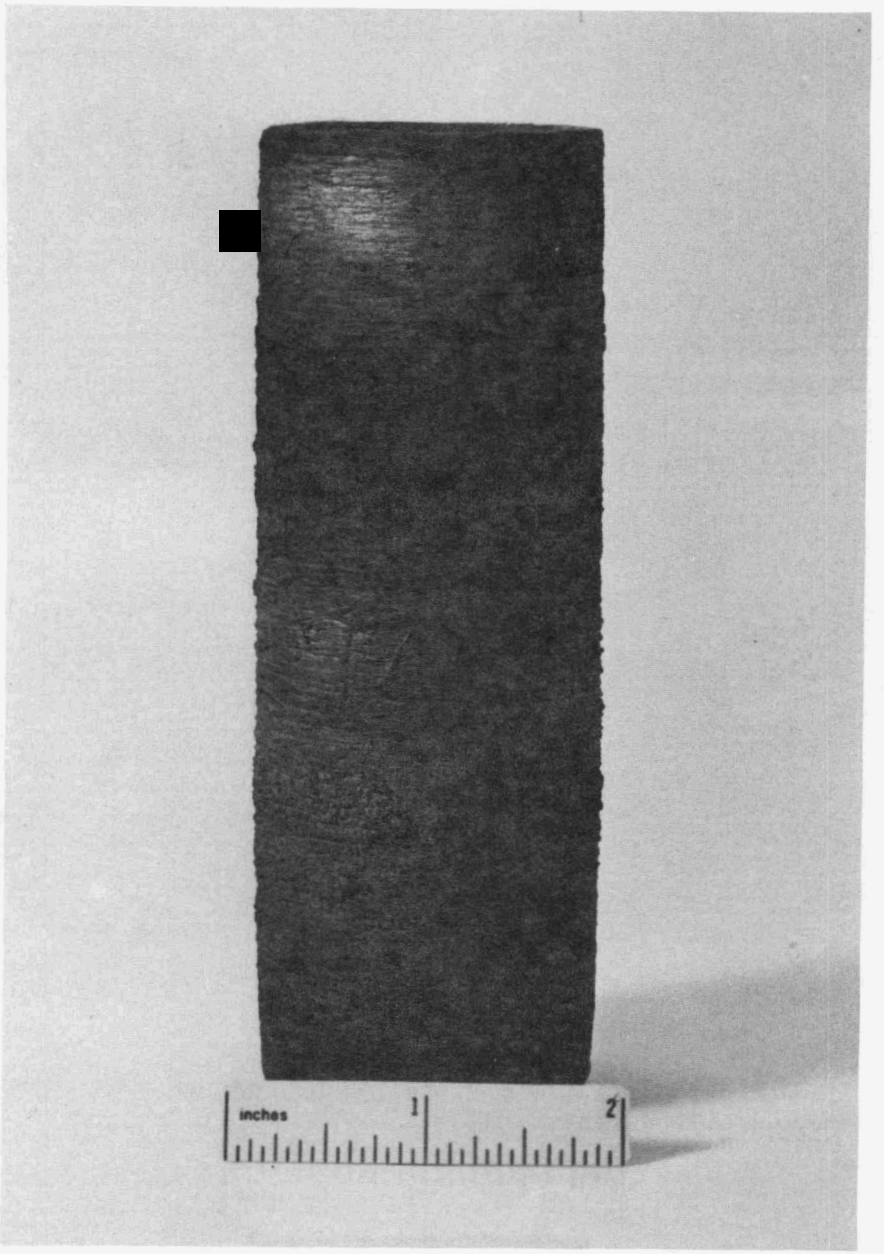

Fig. 8. Infiltrated tube — circumferentially (hoop) wound.

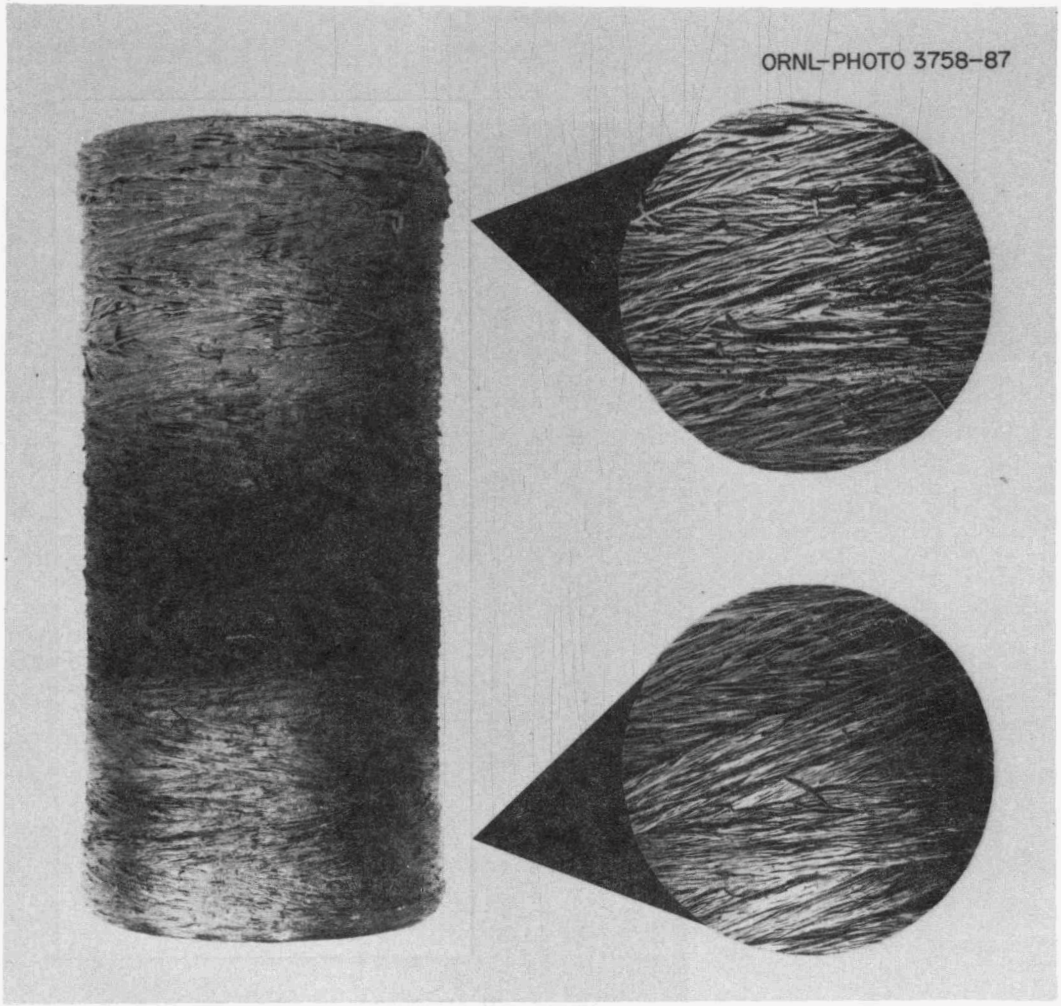

Fig. 9. Infiltrated tube – angle wound with adjacent tows and aligned-tow crossover.

inner preform surfaces. In initial runs, preforms infiltrated using either a graphite mandrel containing only a few holes or slots, a porous carbon mandrel, or no mandrel at all resulted in nonuniform matrix deposition. The best combination of an optimum temperature gradient across the preform wall and uniform-gas flow distribution was obtained with the use of a thin-wall graphite mandrel containing ~200 6-mm-diam (0.25-in.) holes. The multiple axial and radial slots of the distributor are shown in Fig. 4. Less matrix was deposited at the bottom of the preform because of its lower temperature resulting from contact with the base of the cooled graphite gas distributor. To increase the temperature of this area, a ceramic insulator (Si_3N_4-BN) was placed between the bottom of the preform and the cooled distributor base. Ceramographic examination of the longitudinal sections revealed that more-uniform infiltration was obtained with this arrangement. Additional temperature control of the inner and bottom surfaces of the preform was attempted by varying the temperature of the cooling water.

A thermal gradient was not required for the deposition of the pyrolytic carbon precoat. Thus, modifications that removed the cooling of the inside-diameter and bottom surface of the preform were made.

MATRIX DISTRIBUTION

With the use of the multiple-slot graphite gas distributor, the multiple-hole graphite mandrel, and the ceramic insulating spacer at the bottom of the tube, the SiC matrix was deposited rather uniformly across the length and wall thickness of the tube (Fig. 10). A typical, higher-magnification view of the fibers and matrix (Fig. 11) shows that the matrix completely surrounds each fiber. The dark areas in Fig. 11 are pores, which constitute ~15 vol % of this specimen.

Polarized light microscopy was used to distinguish the pyrolytic carbon precoat from the silicon carbide matrix. The carbon thickness varied across both the tube length and wall thickness. The carbon coating thickness from the top to the bottom of the tube at the outer surface varied from 3.5 to 0.5 μm, which was considerably more than the desired 0.1 to 0.2 μm. Figure 12 shows the deposited carbon thicknesses at the outer (2.5-μm) and inner (0.7-μm) tube diameter surfaces.

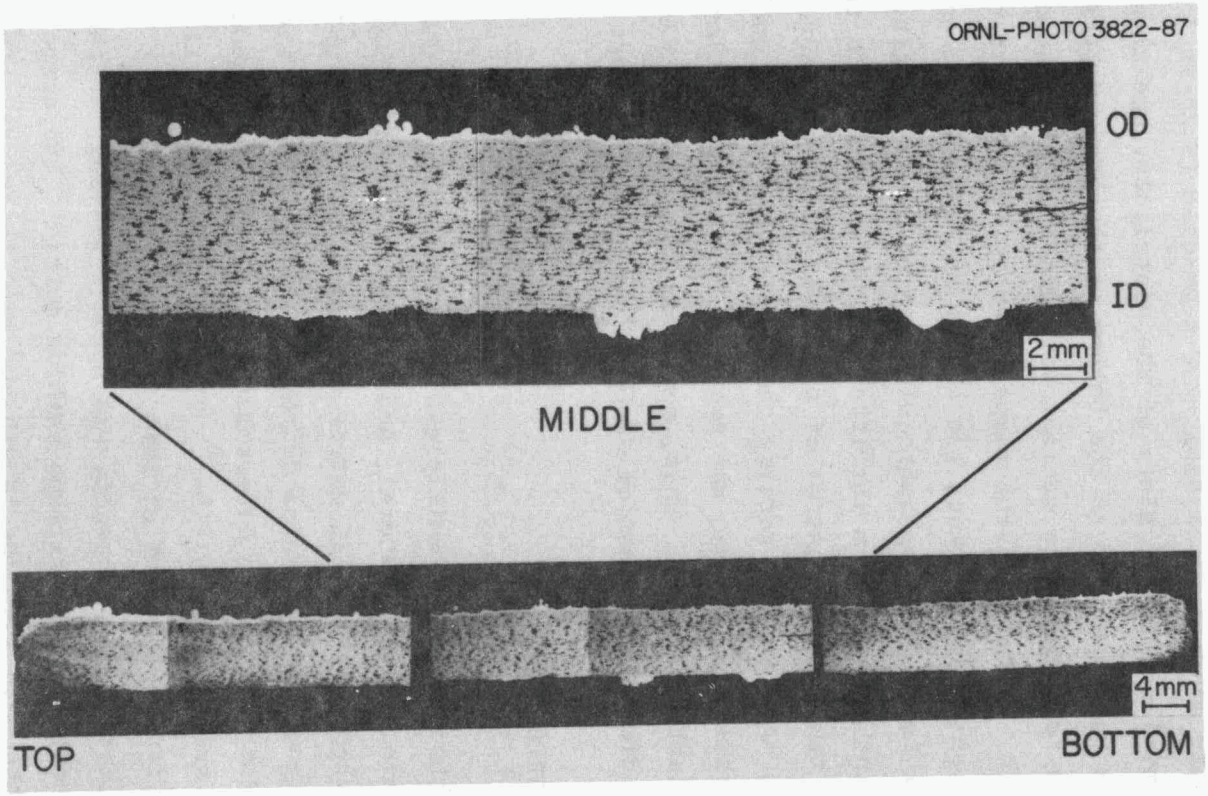

Fig. 10. Matrix was distributed rather uniformly along tube length (run no. 13).

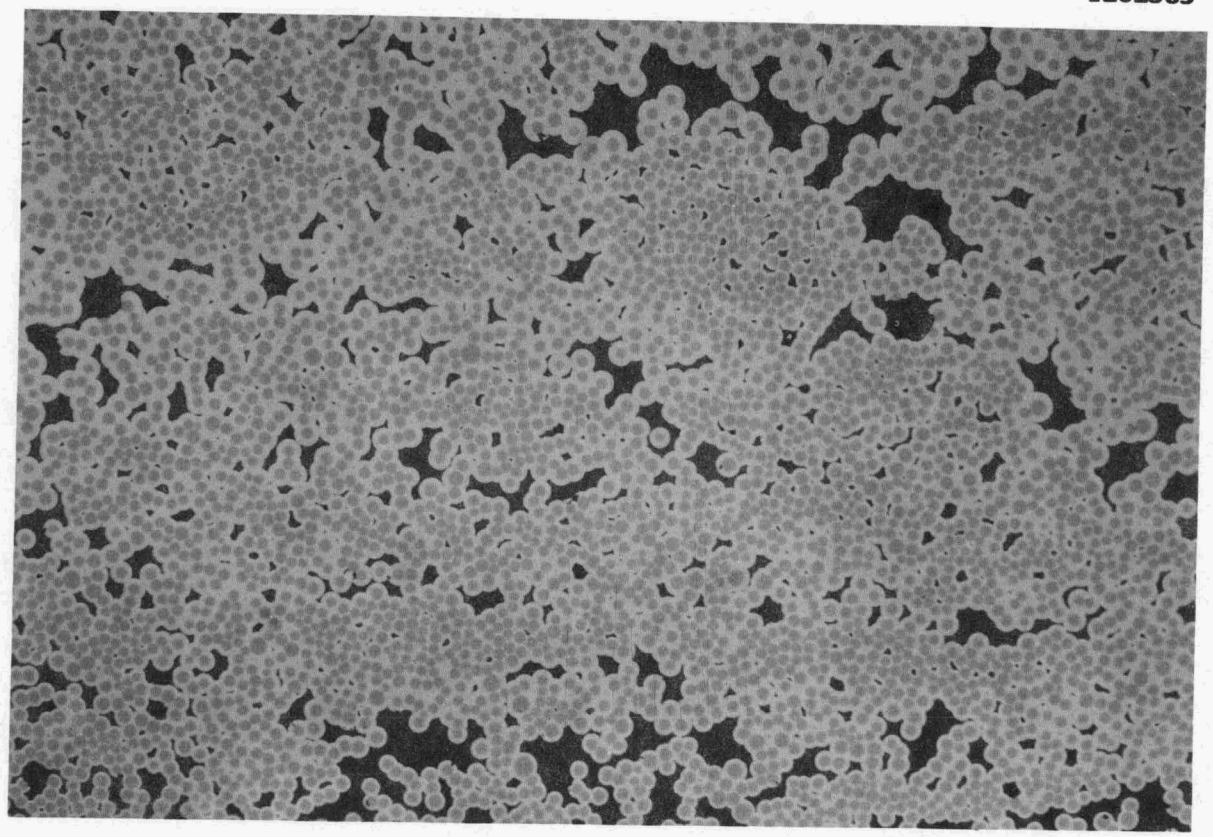

Fig. 11. Typical section of infiltrated silicon carbide fiber-reinforced silicon carbide (run no. 13).

ORNL-PHOTO 3752-87

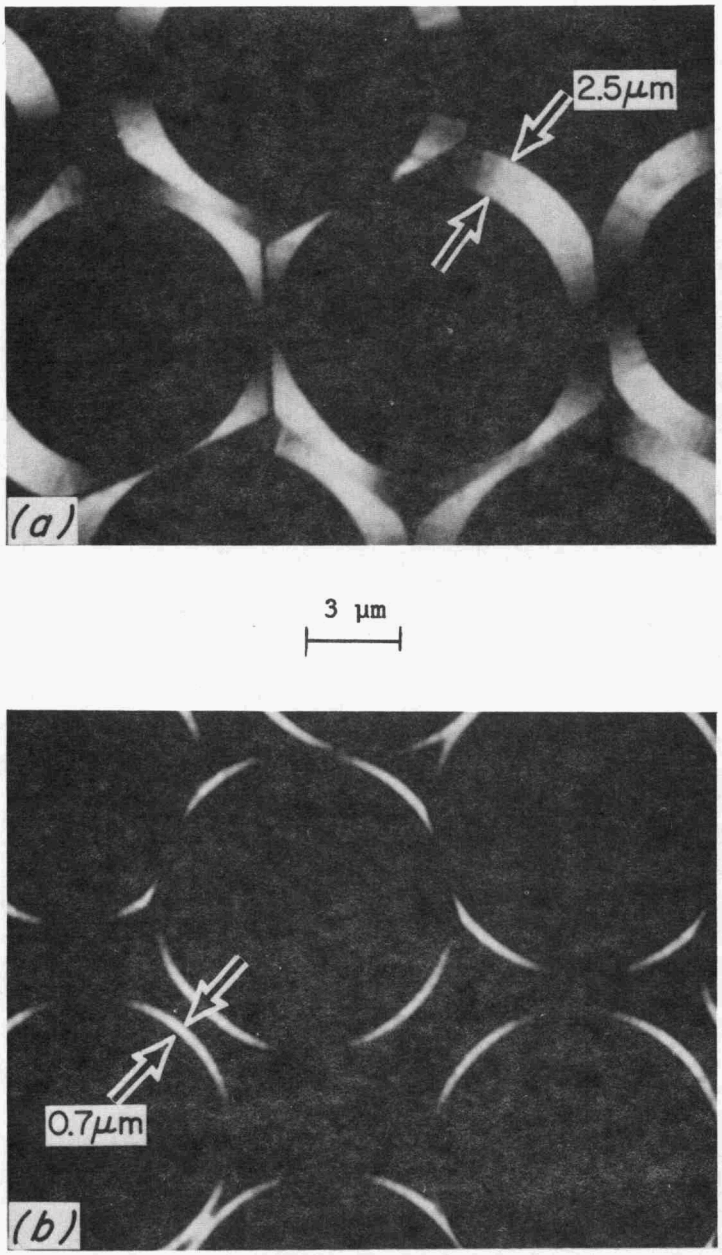

Fig. 12. Pyrolytic carbon coating deposited on SiC fibers before deposition of SiC matrix. (*a*) Middle of tube, OD surface; (*b*) middle of tube, ID surface.

RELATIVE PERMEABILITY

An estimate of the tube room-temperature relative permeability was made before infiltrated tubes 17, 18, and 19 were sectioned (Fig. 13). This was used as an indication of the degree of infiltration. Note that the relative permeability of tubes with a density of ~80% T.D. was nearly identical. A tube with a higher density of ~90% T.D. had a somewhat lower permeability (Fig. 13). Thus, this simple flow test can be used as a first approximation of the relative permeability of the tubes and, for tubes with similar geometry and fabrication history, the degree of infiltration, assuming a uniform matrix distribution.

ROOM-TEMPERATURE TESTING

High-strength, tubular specimens were required to satisfy the goals of this program, however, the load-carrying capability of the composite following initial fracture was also of interest. Therefore, the following were considered in evaluating the specimen:

1. maximum stress at failure,
2. strain to failure, and
3. shape of the stress-strain diagram.

The C-ring specimens, which were loaded in compression, had common failure characteristics. In general, a macrocrack appeared to originate on the outside diameter of the specimen (the tensile surface) and propagate toward the inside diameter. When the crack tip propagated through approximately one-third to one-half of the wall thickness, the crack turned and propagated circumferentially around the tube, causing delamination parallel to the direction of the fiber winding. Although the specimens were cracked after the testing was completed, they remained whole. The segments of the specimens were later separated to examine the fracture surfaces.

The difficulty in interpreting the results of the C-ring test for a delaminating composite is recognized; thus the strengths are reported for comparison rather than as actual tensile strength values. The maximum stress in specimens that were prepared from tubes with fibers wound at 0° in the hoop direction was ~450 MPa (65 ksi). When the reinforcing fiber direction was changed to 10° off the hoop direction, the maximum strength

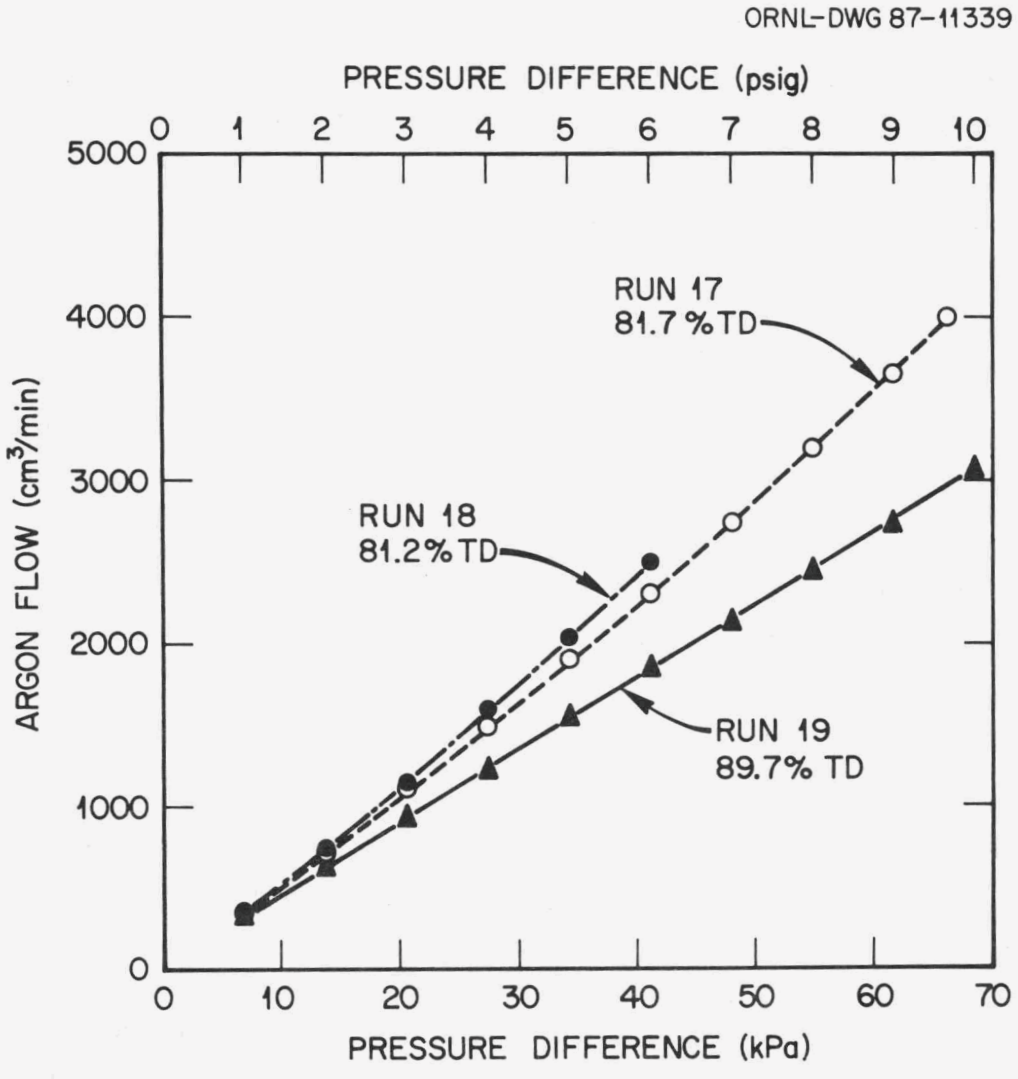

Fig. 13. Room-temperature permeability of infiltrated tubes varied with tube density.

increased to 665 MPa (96 ksi). When pyrolytic carbon was used to precoat the latter preforms, the maximum stress obtained was 810 MPa (118 ksi). These values are substantially higher than the values of 264 to 305 MPa (38 to 44 ksi) for C-rings of monolithic alpha silicon carbide.[24-25]

A prolonged load-carrying capability was observed during the failure of specimens that had densities in the range of 65 to 85% of theoretical, as evidenced in the stress-strain curves produced during testing (Fig. 14). To contrast the difference in the strain to failure of the composite to a monolithic silicon carbide, the failure curve of a monolithic alpha silicon carbide C-ring is also shown. The failure strain of the composite is substantially higher, and the area under the curve is much greater, showing that the toughness of the composite is also greater than that of the unreinforced material (Fig. 14).

The load-carrying capability (composite behavior) after the first indication of cracking can be attributed to fiber pullout during failure. Figures 15 and 16 show fracture surfaces of C-ring specimens tested at room temperature. While delamination of the composites did occur during testing, it is obvious from these photographs that fiber pullout was experienced during fracture.

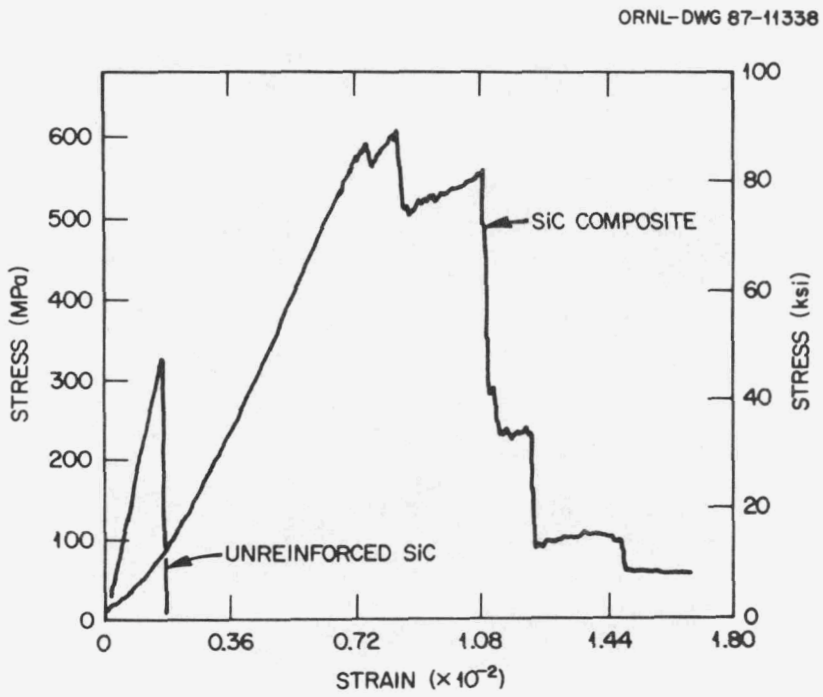

Fig. 14. Stress-strain curve of a specimen fractured at room temperature.

YP6310

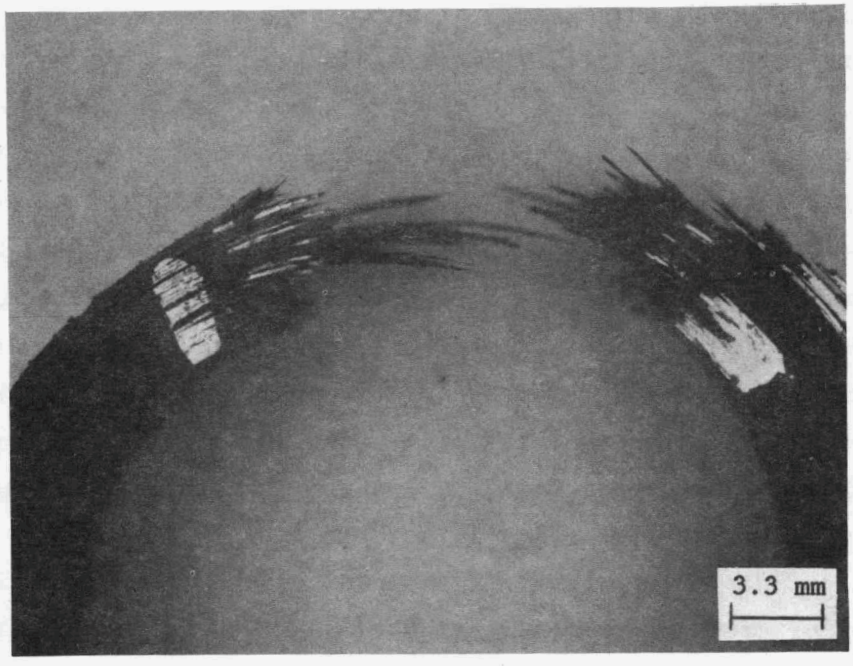

Fig. 15. Fractured C-ring tested at room temperature shows fiber pullout (run no. 17).

ORNL-PHOTO 3756-87

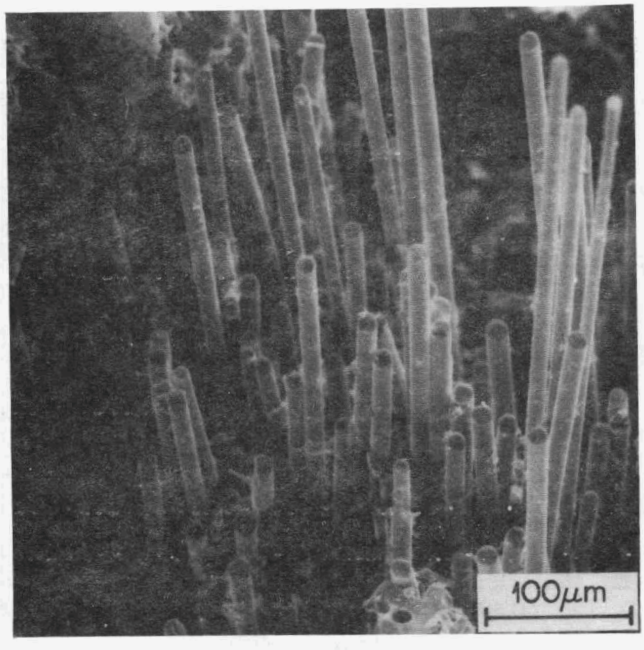

Fig. 16. Fracture surface of a specimen tested at room temperature shows fiber pullout (run no. 17).

Figure 17 shows the fiber-matrix interface of a fracture surface of a composite tube with a pyrolytic carbon precoating. Note the thin layer separating the fiber from the matrix. This layer is believed to contribute to composite behavior by protecting the fibers during processing and weakening the fiber-matrix interfacial bond, although more research will be required to fully delineate its contribution.

ORNL-PHOTO 3754-87

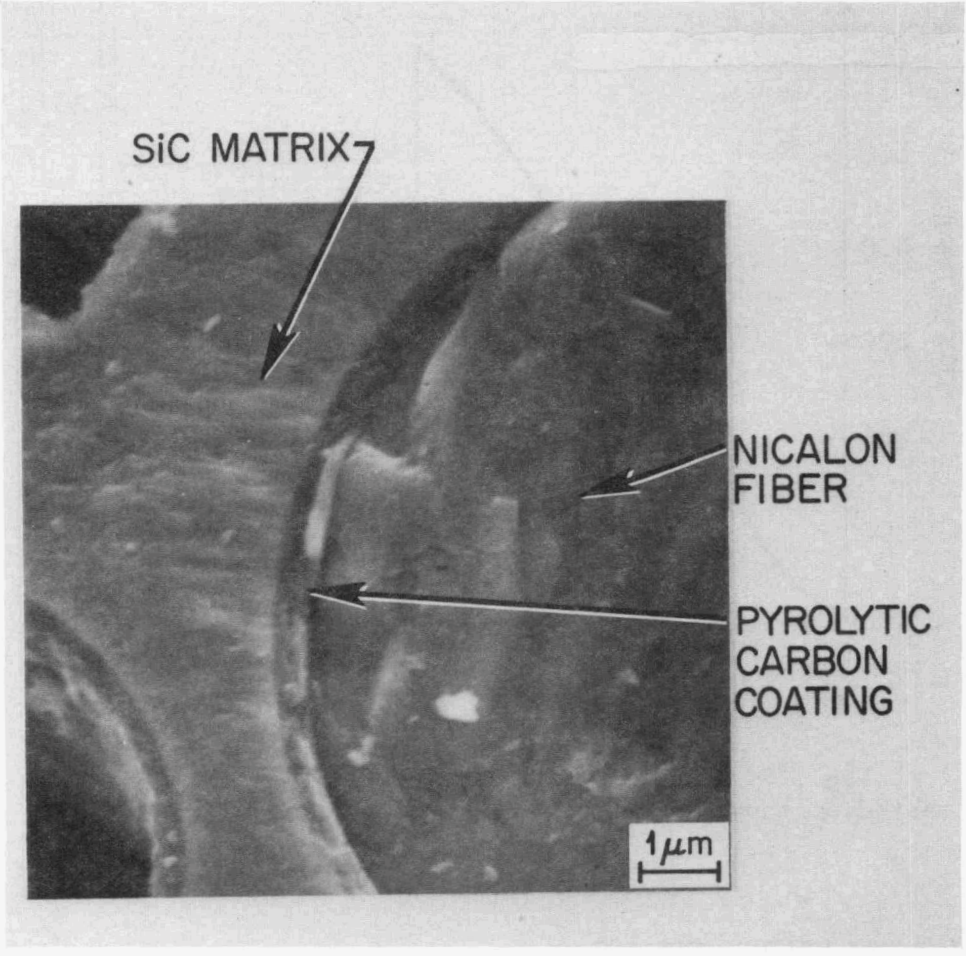

Fig. 17. Fiber-matrix interface of carbon-coated fiber composite following room-temperature tests (run no. 17).

Specimens from run 19 had an average density of 76±4% of theoretical but were not carbon precoated. These specimens did not exhibit composite behavior at room temperature. Figure 18 shows a stress-strain curve of one of the C-ring specimens tested. This curve is more typical of monolithic

ceramic material exhibiting catastrophic failure. The fracture surfaces are irregular, however, which would indicate that some toughening occurred (Fig. 19). Because of the irregular surface and the lack of fiber pullout, it appears that other toughening mechanisms – such as crack deflection and delamination – rather than fiber pullout were present.

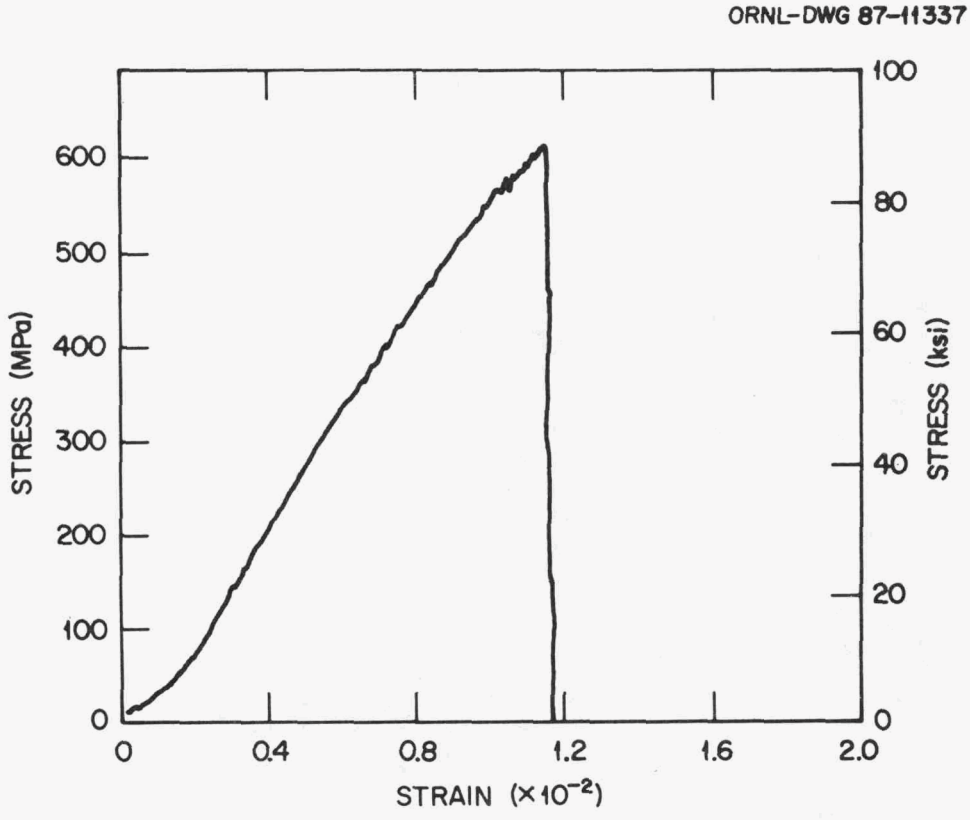

Fig. 18. Stress-strain curve of a 74%-dense specimen tested at room temperature (run no. 19).

ELEVATED-TEMPERATURE TESTING

All tested specimens showed good composite behavior at elevated temperatures. Figure 20 shows a fracture surface of a C-ring specimen tested at 1273 K in air with extensive fiber pullout.

ORNL-PHOTO 3755-87

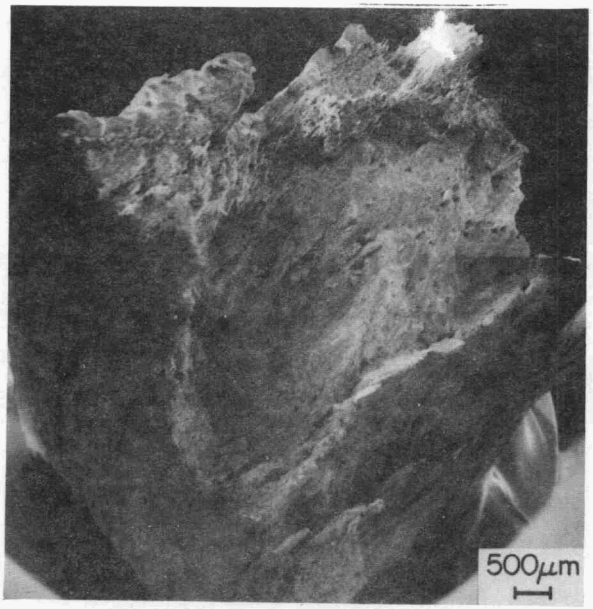

Fig. 19. Fracture surface of a 74%-dense specimen tested at room temperature (run no. 19).

ORNL-PHOTO 3757-87

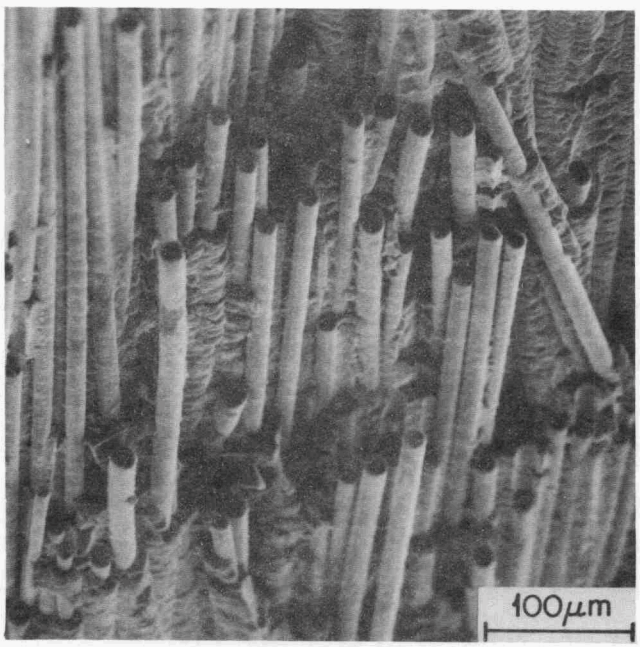

Fig. 20. Fracture surface of a specimen tested at 1273 K in air shows fiber pullout (run no. 19).

In the specimens that were prepared from tubes with fibers wound in the hoop direction, the maximum stress achieved was ~280 MPa (40 ksi). When the reinforcing fiber direction was changed to 10° off the hoop direction, the maximum strength observed was ~415 MPa (60 ksi). When carbon was used to coat the later angle-wound preforms, the maximum stress obtained was 490 MPa (71 ksi) (Table 3).

Figure 21 shows fracture surfaces of specimens that had a carbon precoat and were tested at 1273K. It was assumed that the carbon coating would be vulnerable in an oxidizing environment, particularly following cracking of the matrix. Figure 21(*a*) shows an area of the fracture surface in which the carbon coating remained. However, Fig. 21(*b*) shows an area of the same fractured surface in which no carbon coating remained, and Fig. 21(*c*) shows an area where fibers were partly coated with carbon. These results indicate that the matrix protected the carbon coating interface for a limited time at 1273 K.

The specimens cut from the composite tube that had an average infiltrated density of 90% of theoretical also exhibited composite behavior at elevated temperature, as evidenced by the stress-strain curves shown in Figs. 22 and 23. Figure 22 was generated during a specimen test at 1273 K, and Fig. 23 was generated during a specimen test at 1473 K. At 1473 K the specimens exhibited strengths of ~172 MPa (25 ksi) and good composite behavior.

DISCUSSION

Ceramic tubular composites fabricated utilizing CVI techniques have been examined for applications as high-temperature heat exchanger components in industrial processes.[28] Braided fiber tubing has been infiltrated with silicon carbide to produce thermal shock resistant composites which offer great potential as heat pipes, nozzles, and other combustion system components. Siconex, a trademark of 3M, are composites composed of Nextel alumino-borosilicate fibers densified with a CVI SiC matrix. The investigation of these materials has been limited to thin wall (single layer) structures and the products possess very low strength, typically <70 MPa compressive. These strengths are adequate for nonstructural heat exchanger components; however, improved properties are required for the more demanding applications.

ORNL-PHOTO 3753-87

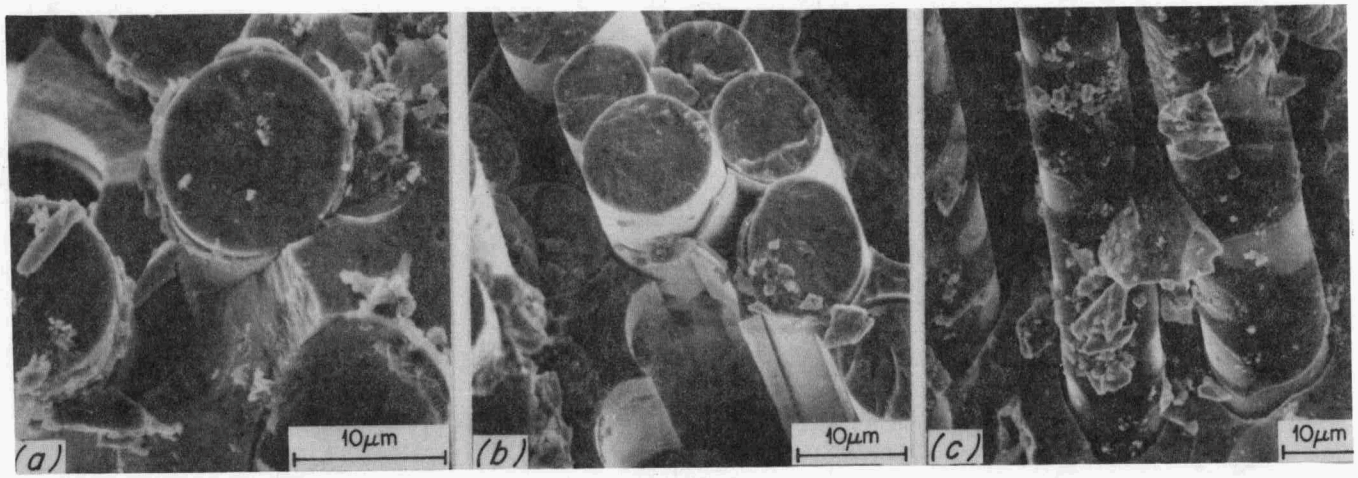

Fig. 21. Fiber-matrix interface of carbon-coated fiber composite tested at 1000°C. (*a*) Area showing fibers with carbon coating, (*b*) area showing fibers with no carbon coating, (*c*) area showing fibers partly coated with carbon (run no. 18).

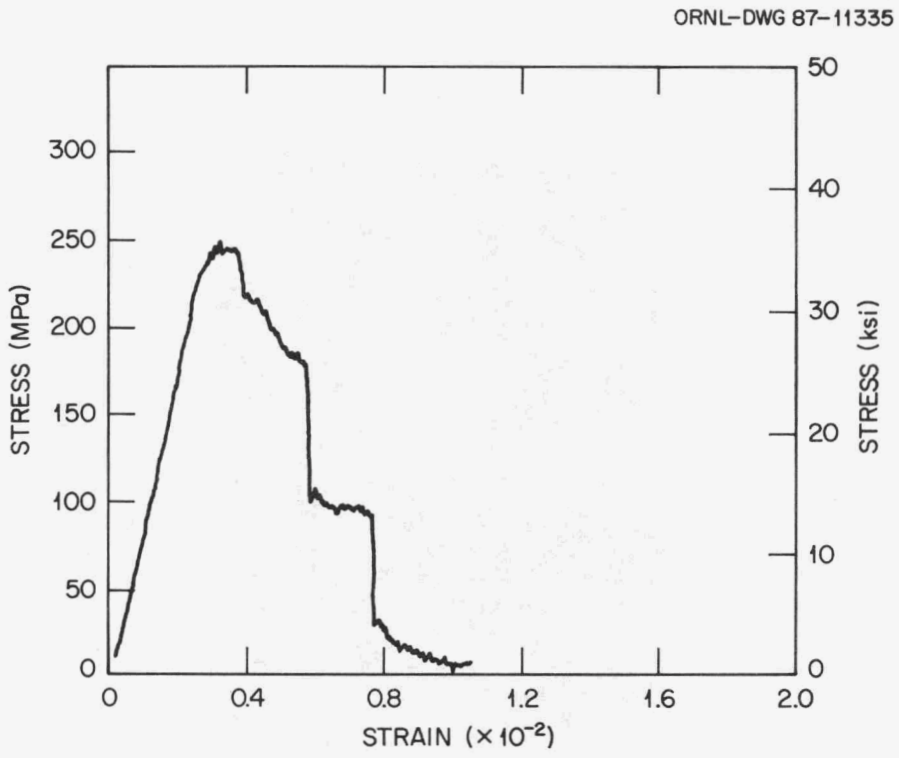

Fig. 22. Stress-strain curve of a 79%-dense specimen tested at 1273 K in air (run no. 19).

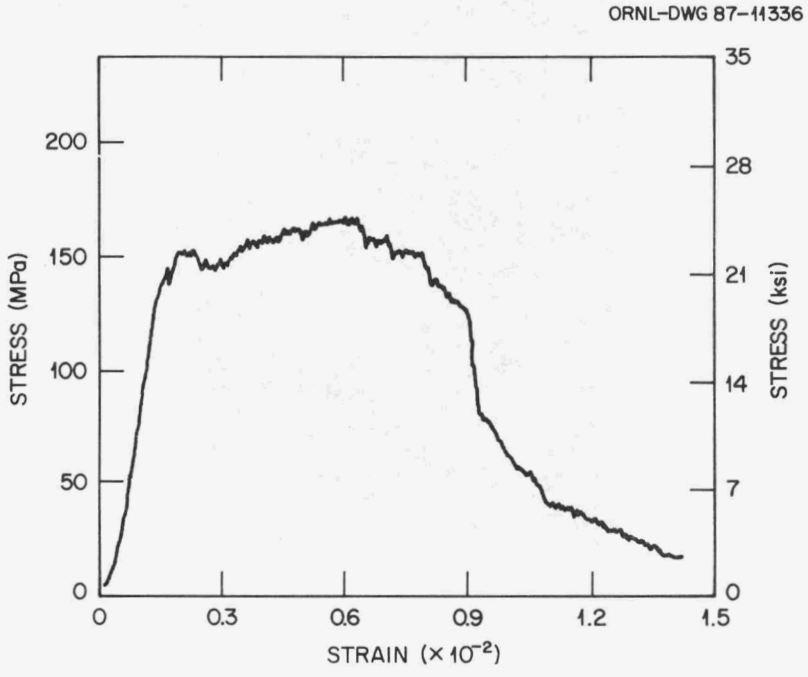

Fig. 23. Stress-strain curve of a 76%-dense specimen tested at 1473 K in air (run no. 19).

High strength composites with improved toughness have been produced utilizing the forced-flow, thermal-gradient CVI process developed at ORNL. In contrast to the braided single-layer preforms densified in the aforementioned programs, relatively thick, filament-wound structures have been infiltrated with a SiC matrix. The process utilizes both the thermal-gradient and forced-flow approaches to significantly reduce processing times. Composite tubes containing a nominal 50 vol. % fiber have been infiltrated to 90% of theoretical density in <65 h.

Numerous factors influence the infiltration process. An adequate temperature gradient must be retained and the reactant gases must be evenly distributed to produce a composite with uniform density and properties. The water-cooled injector and the graphite distributor and mandrel played key roles in the infiltration of the fibrous tubes. While adjustment of the water temperature from 290 to 350 K flowing through the metal injector appeared to have little effect on the thermal gradient, the configuration of the mandrel and graphite gas distributor had a significant influence on the temperature distribution throughout the preform.

If the inside surface of the preform was too hot, deposition occurred on this surface sealing it, thus the reactant could not penetrate the remainder of the preform. Too much cooling to the inner diameter, and subsequently the bottom of the preform, did not allow for complete infiltration of the inner and bottom volumes. Reactant gases would simply flow out the cooled bottom edge of the preform that was in contact with the base of the graphite gas distributor. It was found that a ceramic spacer, placed between the gas distibutor and preform, was needed to create the proper temperature gradient for satisfactory infiltration.

The distribution of reactant gases within the preform greatly influenced densification uniformity. A variety of porous mandrels placed between the fibrous preform and the gas distributor were examined. These controlled not only the gas flow but the nature of the thermal gradient. A graphite mandrel with a series of 6-mm holes was found to be the most efficient. The structure of the preform had the most significant effect on matrix distribution. The filaments in the preforms wound at 0° to the hoop align next to and above one another and thus they create a tortuous

and restrictive path for the reactants. Angular winding of the fiber tows produced preforms with porosity and open passages that permitted the gases to flow more easily from the inner surface to the heated outer areas. This improved infiltration uniformity and thus composite mechanical properties were improved.

The problems associated with the mechanical property testing of composite specimens is recognized and the reported strengths are used for intercomparison rather than true values of tensile strength. The composite specimens delaminated during C-ring testing. Cracks propagating from the outer diameter were quickly diverted around the circumference of the test specimen. The lower density areas at the inner surface of the C-ring may have also influenced results. However, high strengths were measured at room and elevated temperatures. Typical flexure strengths for Nicalon/SiC composites have been reported to be 400-450 MPa from room temperature to 1573 K.[6] Room temperature strengths of ~640 MPa and 1273 K strengths of >300 MPa are respectible. In addition, gradual failure and fiber pull-out were observed in the majority of the specimens.

The winding angle appeared to influence the ultimate strength of the composites. Higher C-ring stengths were measured for the samples fabricated from preforms wound at 10° off the hoop direction than for the 0° windings. In general, the strength of a composite decreases as the angle between the loading direction and filament direction increases. In this case however, the angular winding allowed for more complete and uniform infiltration, and thus an improvement in composite quality.

It was recognized that an intermediate coating applied to the fibers prior to infiltration was necessary to increase strength and improve reproducibility. Carbon has successfully been used an interlayer in SiC/Nicalon composites in the past, and thus a thin layer of carbon was used to protect the fibers from damage during processing and to alter the characteristics of the fiber-matrix interface. Composites fabricated from carbon-coated preforms exhibited improved strength and increased strain-to-failure accompanied by extensive fiber pull-out.

Boron nitride has also been successfully used as a modifying interlayer in composite materials.[30] Continuous fibers with a thin layer of

boron nitride deposited at a low temperature was purchased and wound to form a tube. The tube was densified with SiC and the infiltrated composite specimens exhibited composite failure, but low strengths (run no. 11). The BN interlayer could not be detected in the finished composites suggesting possible chemical interaction with the fiber or the matrix during densification.

CONCLUSIONS

This project demonstrated that the forced-flow, thermal-gradient chemical vapor infiltration process can be used to fabricate tubular composites. Net-shape fibrous structures were prepared by the filament winding of continuous tows. The preforms were densified with a silicon carbide matrix and the properties of the composites were measured.

Tubes with ~6-mm-wall thicknesses were produced in <65 h with densities approaching 90% theoretical. The highest density composites were fabricated from preforms with fibers wound 10° off the hoop direction. The angular winding provided more readily accessible gas passages than did preforms wound at 0° to the hoop direction. The improvements in product density and matrix distribution resulted in an increase in the C-ring strength of the composites. The maximum strength obtained in the tested composites was 810 MPa at room temperature, 490 MPa at 1273 K, and 172 MPa at 1473 K. In general, the composite specimens failed gradually with evidence of fiber pull-out at the fracture surfaces.

A carbon coating applied to the preforms prior to infiltration improved the mechanical behavior of the composites. The carbon alters the bonding characteristics at the fiber-matrix interface and helps to protect the fibers from damage during processing. A BN coating deposited on the fibers before filament winding appeared to have a deleterious effect on the properties of the composite.

ACKNOWLEDGMENT

The authors acknowledge J. I. Federer and G. L. Copeland, (Oak Ridge National Laboratory) and W. G. Long (Babcock and Wilcox) for review of the draft report. The authors with to thank C. A. Valentine for typing the draft report, S. R. Parker for editing, and M. R. Upton and G. R. Carter for preparing the final manuscript.

REFERENCES

1. K. M. Prewo and J. J. Brennan, "High-Strength Silicon Carbide Fiber-Reinforced Glass-Matrix," *J. Mat. Sci.* **15**, 463–68 (1980).

2. K. M. Prewo and J. J. Brennan, "Silicon Carbide Yarn Reinforced Glass Matrix Composites," *J. Mat. Sci.* **17**, 1201–6 (1982).

3. J. J. Brennan and K. M. Prewo, "Silicon Carbide Fiber-Reinforced Glass-Ceramic Matrix Composites Exhibiting High Strength and Toughness," *J. Mat. Sci.* **17**, 2371–83 (1982).

4. E. Fitzer, D. Hegen, and H. Strohmeier, "Chemical Vapor Deposition of Silicon Carbide and Silicon Nitride and Its Application for Preparation of Improved Silicon Ceramics," pp. 525–35 in *Proc. Seventh Int'l Conf. Chem. Vapor Dep.*, ed. T. D. Sedgwick and H. Hydtin, Electrochemical Society, Princeton, N.J., 1979.

5. G. C. Wei and P. F. Becher, "Development of SiC-Whisker-Reinforced Ceramics," *Am. Ceram. Soc. Bull.* **64**(2), 298–304 (1985).

6. P. J. Lamicq et al., "SiC/SiC Composite Ceramics," *Am. Ceram. Soc. Bull.* **65**(2), 336–38 (1986).

7. J. A. Cornie et al., "Processing of Metal and Ceramic Matrix Composites," *Am. Ceram. Soc. Bull.* **65**(2), 293–304 (1986).

8. W. H. Pfeifer et al., "Consolidation of Composite Structures by CVD," pp. 463–83 in *Second Int'l Conf. Chem. Vapor Dep.*, ed. J. M. Blocher, Jr., and J. C. Withers, Electrochemical Society, New York, 1970.

9. J. C. Withers, "Chemical Vapor Deposition of Ceramic Composites Containing Whisker and Fiber Reinforcements," pp. 507–19, in *Second Int'l Conf. Chem. Vapor Dep.*, ed. J. M. Blocher, Jr., and J. C. Withers, Electrochemical Society, New York, 1970.

10. J. D. Theis, Jr., "The Process Development and Mechanical Testing of a Carbon/Carbon Composite Fabricated by Chemical Vapor Infiltration of a Filament-Wound Substrate," pp. 561–73 in *Third Int'l Conf. Chem. Vapor Dep.*, ed. F. A. Glaski, American Nuclear Society, Hinsdale, Ill., 1972.

11. L. R. Newkirk et al., "Chemical Vapor Deposition Fabrication of Filament-Reinforced Composites for High Temperature Applications," pp. 82–101 in *Chemically Vapor Deposited Coatings*, ed. H. O. Pierson, American Ceramic Society, Columbus, Ohio, 1981.

12. J. J. Gebhardt, "CVD Boron Nitride Infiltration of Fibrous Structures: Properties of Low Temperature Deposits," pp. 460–72 in *Fourth Int'l Conf. Chem. Vapor Dep.*, ed. G. F. Wakefield and J. M. Blocher, Jr., Electrochemical Society, Princeton, N.J., 1973.

13. F. Christin, R. Naslain, and C. Bernard,"A Thermodynamic and Experimental Approach of Silicon Carbide-CVD Application to the CVD-Infiltration of Porous Carbon-Carbon Composites," pp. 499–514 in *Proc. Seventh Int'l Conf. Chem. Vapor Dep.*, ed. T. O. Sedgwick, amd H. Hydtin, Electrochemical Society, Princeton, N.J., 1979.

14. R. Naslain, et al, "Chemical Vapor Infiltration Technique," pp. 293–304 in *Proceedings of the Fourth European Conference on Chemical Vapor Deposition*, ed. J. Bloem, G. Verspul, L. R. Wolff, Philips Centre for Manufacturing Technology, Eindhoven, Netherlands, 1983.

15. A. J. Caputo and W. J. Lackey, *Fabrication of Fiber-Reinforced Ceramic Composites by Chemical Vapor Infiltration*, ORNL/TM-9235, October 1984.

16. A. J. Caputo and W. J. Lackey, "Fabrication of Fiber-Reinforced Ceramic Composites by Chemical Vapor Infiltration," *Ceram. Eng. & Sci. Proc.* 5(7–8), 654–67 (1984).

17. A. J. Caputo, W. J. Lackey, and D. P. Stinton, "Development of a New, Faster Process for the Fabrication of Ceramic Fiber-Reinforced Ceramic Composites by Chemical Vapor Infiltration," *Ceram. Eng. & Sci. Proc.* 6(7–8), 694–706 (1985).

18. A. J. Caputo, R. A. Lowden, and D. P. Stinton, *Improvements in the Fabrication of Ceramic-Fiber-Ceramic-Matrix Composites by Chemical Vapor Deposition*, ORNL/TM-9651, June 1985.

19. D. P. Stinton, A. J. Caputo, and R. A. Lowden, "Synthesis of Fiber-Reinforced SiC Composites by Chemical Vapor Infiltration, *Am. Ceram. Soc. Bull.* 65(2), 347–50 (1986).

20. A. J. Caputo, R. A. Lowden, and D. P. Stinton, "Fiber-Reinforced SiC Composites with Improved Mechanical Properties," *Am. Ceram. Soc. Bull.* 66(2), 368–72 (1987).

21. A. J. Caputo and W. J. Lackey, Process for the Preparation of Fiber-Reinforced Ceramic Composited by Chemical Vapor Deposition, U.S. patent 4,580,524, April 8, 1986.

22. E. P. Popov, *Mechanism of Materials*, 2d ed., Prentice-Hall, Inc., Englewood Cliffs, N.J., 1976, pp. 150–55.

23. J. N. Cernica, *Strength of Materials*, Holt, Rinehart and Winston, Inc., New York, 1966, pp. 201–05.

24. M. K. Ferber and V. J. Tennery, *Evaluation of Tubular Ceramic Heat Exchanger Materials in Acidic Coal Ash from Coal-Oil-Mixture Combustion*, ORNL/TM-7958, December 1981.

25. M. K. Ferber and V. J. Tennery, *Evaluation of Tubular Ceramic Heat Exchanger Materials in Basic Coal Ash from Coal-Oil-Mixture Combustion*, ORNL/TM-8385, October 1982.

26. T. S. Brown, Research and Development Div., Babcock and Wilcox, Alliance, Ohio, letter to H. H. Moeller, Lynchburg Research Center, Babcock and Wilcox, Lynchburg, Va., March 28, 1986.

27. F. B. Seely and J. O. Smith, *Advanced Mechanics of Materials*, 2d ed., John Wiley and Sons, New York, pp. 167–74.

28. P. Reagan, W. Cole, and F. Huffman, "CVD Silicon Carbide Components," *Ceram. Eng. Sci. Proc.* **8**(7–8), 958-67 (1987).

29. W. E. Cole, et al., "Ceramic Composite Heat Exchangers," *Ceram. Eng. Sci. Proc.* **8**(7–8), 968-75 (1987).

30. R. W. Rice, et al., "The Effect of Fiber Coatings on the Room-Temperature Behavior of Ceramic-Fiber Composites," *Ceram. Eng. Sci. Proc.* **2**(7–8), 661-701 (1981).

INTERNAL DISTRIBUTION

1–2. Central Research Library
3. Document Reference Section
4–5. Laboratory Records Department
6. Laboratory Records, ORNL RC
7. ORNL Patent Section
8–10. M&C Records Office
11. P. Angelini
12. R. L. Beatty
13. P. F. Becher
14. T. M. Besmann
15. P. J. Blau
16. A. Bleier
17. E. E. Bloom
18. R. A. Bradley
19. C. R. Brinkman
20–24. A. J. Caputo
25. P. T. Carlson
26. R. H. Cooper
27. D. F. Craig
28. R. S. Holcomb
29. C. H. Hsueh
30. D. R. Johnson
31. R. R. Judkins
32. E. L. Long, Jr.
33–37. R. A. Lowden
38. T. S. Lundy
39. A. C. Schaffhauser
40. M. Siman-Tov
41. D. P. Stinton
42. J. R. Weir, Jr.
43. A. D. Brailsford (Consultant)
44. H. D. Brody (Consultant)
45. F. F. Lange (Consultant)
46. D. P. Pope (Consultant)
47. E. R. Thompson (Consultant
48. J. B. Wachtman, Jr. (Consultant)

EXTERNAL DISTRIBUTION

49. ACUREX CORPORATION, 555 Clyde Avenue, P.O. Box 7555, Mountain View, CA 94039

    J. Sawyer

50. ADIABATICS, INCORPORATED, 630 S. Mapleton, Columbus, IN 47201

    Roy Kamo, President

51–52. AFWAL/MLLM, Wright-Patterson AFB, OH 45433

    Alan Katz
    S. Szaruga

53–56. AIR PRODUCTS AND CHEMICALS, INC., P.O. Box 538T, Allentown, PA 18105

    P. N. Dyer
    V. L. Magnotta
    R. K. Malhotra
    S. V. Raman

57. AIRCO TEMESCAL, 2850 Seventh Street at Heinz, Berkeley, CA 94710

    Ernest Demiray

58. AIRESEARCH MANUFACTURING COMPANY, 2525-T West 190th Street, Torrance, CA 90509

    D. M. Kotchick

59. AMERCOM, INC., 8928 Fullbright Avenue, Chatsworth, CA 91311

W. E. Bustamante

60. ARCO CHEMICALS COMPANY, Silag Operation, Route 6, Box A, Greer, SC 29651

J. F. Rhodes

61. ARGONNE NATIONAL LABORATORY, 9700 South Cass Avenue, Argonne, IL 60439

W. A. Ellingson

62-63. ARMY MATERIALS AND MECHANICS RESEARCH CENTER, Arsenal Street, Watertown, MA 02172

R. N. Katz
J. W. McCauley

64. AVCO, 201 Lowell Street, Wilmington, MA 01887

Tom Vasilos

65-68. AVCO SPECIALTY MATERIALS, 2 Industrial Avenue, Lowell, MA 01851

B. Belason
T. F. Foltz
W. Foulds
J. F. Lacouste

69-76. BABCOCK & WILCOX COMPANY, Lynchburg Research Center, P.O. Box 239, Lynchburg, VA 24505

L. J. Ferrell
W. G. Long
H. H. Moeller (5)
D. R. Petrak

77-78. BATTELLE COLUMBUS LABORATORIES, 505 King Avenue, Columbus, OH 43201

S. P. Mukherjee
I. G. Wright

79-82. BATTELLE PACIFIC NORTHWEST LABORATORIES, P.O. Box 999, Battelle Boulevard, Richland, WA 99352

Ed Cartwright
T. D. Chikalla
S. D. Dahlgren
Ed McClanahan

83. CABOT CORPORATION, 125 High Street, Boston, MA 02110

Nicholas Fiore

84-86. CATERPILLAR TRACTOR COMPANY, Peoria, IL 61629

M. B. Beardsky
M. Haselkorn
G. G. Volbert

87-88. CERAMATEC, INC., 163 West 1700 Street, Salt Lake City, UT 84115

C. W. Griffin
D. W. Richerson

89–92. CORNING GLASS WORKS, Corning, NY 14831

K. Chyung
R. C. Doman
D. C. Larson
P. Papa

93–95. CUMMINS ENGINE COMPANY, INC., 1000 5th St., Columbus, IN 47201

J. W. Patten
G. L. Starr
T. M. Yonushonis

96. DOW CORNING CORPORATION, 3901 South Saginaw Road, Midland, MI 48640

H. W. Foglesong

97–98. E. I. DUPONT DE NEMOURS & COMPANY, INC., Experimental Station 302/22, Wilmington, DE 19898

P. Geoghegan
J. C. Romine

99–100. FORD MOTOR COMPANY, Engineering and Research, P.O. Box 2053, Dearborn, MI 48121

D. L. Hartsock
A. F. McLean

101–102. GA TECHNOLOGIES, INC, P.O. Box 81608, San Diego, CA 92138

T. D. Gulden
K. S. Mazdiyasni

103. GENERAL MOTORS CORPORATION, Allison Gas Turbine Operations, Low Heat Rejection Diesel Technology, P.O. Box 420, Indianapolis, IN 46206

H. E. Helms

104–105. GEORGIA INSTITUTE OF TECHNOLOGY, 225 North Avenue, Atlanta, GA 30332

W. J. Lackey
T. L. Starr

106–108. GTE LABORATORIES, INC., 40 Sylvan Road, Waltham, MA 02254

M. L. Huckabee
A. E. Pasto
V. Sarin

109. HUGHES AIRCRAFT COMPANY, P.O. Box 902, 2000 East El Segundo Boulevard, El Segundo, CA 90245

Mike Gardos

110. KAMAN SCIENCES CORPORATION, 1500 Garden of the Gods Road, P.O. Box 7463, Colorado Springs, CO 80933

J. L. Carr

111–112. KENNAMETAL, INC., P.O. Box 231, Latrobe, PA 15650

D. Kropful
E. J. Oles

113. KRW ENERGY SYSTEMS, P.O. Box 158, Madison, PA 15663

C. A. Andersson, Jr.

114-116. LANXIDE CORPORATION, Tralee Industrial Park, Newark, DE 19711

V. Irick, Jr.
M. Newkirk
A. W. Urquhart

117-119. LAWRENCE BERKELEY LABORATORY, University of California, P.O. Box 808, 1 Cyclotron Road, Berkeley, CA 94720

D. H. Boone
A. G. Evans
A. V. Levy

120-122. LOS ALAMOS NATIONAL LABORATORY, P.O. Box 1663, Los Alamos, NM 87545

F. D. Gac
G. F. Hurley
J. J. Petrovic

123-124. MARTIN MARIETTA LABORATORIES, 1450 South Rolling Road, Baltimore, MD 21227

D. C. Nagle
A. R. C. Westwood

125-126. MASSACHUSETTS INSTITUTE OF TECHNOLOGY, Cambridge, MA 02139

H. K. Bowen
J. S. Haggerty

127-128. MECHANICAL TECHNOLOGY, INC., 968 Albany-Shaker Road, Latham, NY 12110

W. F. Bessler
M. Schreiner

129. NASA-LANGLEY RESEARCH CENTER, MS 188-B, Hampton, VA 23665

D. R. Tenney

130-135. NASA-LEWIS RESEARCH CENTER, 21000 Brookpark Road, Cleveland, OH 44135

C. C. Berndt
D. H. Buckley
S. R. Levine
T. J. Miller
H. B. Probst
Harold Sliney

136. NATIONAL ACADEMY OF SCIENCES, National Materials Advisory Board, Washington, DC 20418

R. M. Spriggs

137–138. NATIONAL BUREAU OF STANDARDS, 562 Fracture and Deformation, Gaithersburg, MD 20899

E. R. Fuller
S. M. Wiederhorn

139. NATIONAL RESEARCH COUNCIL OF CANADA, 1411 Oxford Street, Halifax, N.S., Canada B3H3Z1

K. J. Konsztowicz

140–141. NORTH CAROLINA STATE UNIVERSITY, Department of Materials Engineering, P.O. Box 5427, 232 Riddick Laboratory, Raleigh, NC 27607

Hans Conrad
R. F. Davis

142. NORTH CAROLINA STATE UNIVERSITY, P.O. Box 5995, Raleigh, NC 27607

H. Palmour III

143. OAK RIDGE ASSOCIATED UNIVERSITIES LIBRARY, Oak Ridge, TN 37831

MERT Division

144. OHIO STATE UNIVERSITY, 2041 College Road, Columbus, OH 43210

Dennis Readey

145–146. PENNSYLVANIA STATE UNIVERSITY, Materials Engineering Research Laboratory, 201 Steidle Building, University Park, PA 16802

Karl Spear
R. E. Tressler

147–149. PRATT & WHITNEY AIRCRAFT, 400 Main St., East Hartford, CT 06108

O. Chen
C. S. Giggins
D. L. Ruckle

150. REFRACTORY COMPOSITES, INC., 12220-A Rivera Road, Whittier, CA 90606

E. Paquette

151. ROCKWELL INTERNATIONAL, 1049 Camino Dos Rios, P.O. Box 1085, Thousand Oaks, CA 91360

P. E. D. Morgan

152. SAN FERNANDO LABORATORIES, 10258 Norris Avenue, Pacoima, CA 91331

R. A. Holzl

153. SANDIA NATIONAL LABORATORIES, P.O. Box 5800, Albuquerque, NM 87115

Donald Maddox

154. R. L. Smith, P.O. Box 98, Chassel, MI 49916

155. TECHNOLOGY ASSESSMENT AND TRANSFER COMPANY, 9607 Muirfield Drive, Upper Marlboro, MD 20772

L. L. Fehrenbacher

156. 3M COMPANY, 3M Center, 218-35-04, St. Paul, MN 55144

R. E. Richards

157. UNION CARBIDE CORPORATION, Market Development, Carbon Products Division, P.O. Box 6087, Cleveland, OH 44101

M. B. Dowell

158. U.S. ARMY TANK-AUTOMOTIVE COMMAND (TACOM), R&D Center, Warren, MI 48090

P. C. Glance

159. U.S. DEPARTMENT OF DEFENSE, Advanced Research Projects Agency, 1400 Wilson Boulevard, Arlington, VA 22209

B. F. Wilcox

160-161. UNITED TECHNOLOGIES RESEARCH CENTER, Silver Lane, MS 24, East Hartford, CT 06108

J. J. Brennan
Karl Prewo

162. UNIVERSITY OF TENNESSEE, Department of Materials Science, Knoxville, TN 37996

J. E. Spruill

163. UNIVERSITY OF WASHINGTON, Seattle, WA 98195

R. C. Bradt

164. VIRGINIA POLYTECHNIC INSTITUTE AND STATE UNIVERSITY, Blacksburg, VA 24061

D. P. H. Hasselman

165. VOUGHT CORPORATION, MSTH 83, P.O. Box 225907, Dallas, TX 75265

H. F. Volk

166-167. W. R. GRACE & COMPANY, 7379 Route 32, Columbia, MD 21044

R. W. Rice
J. P. Skalny

168. WESTINGHOUSE ELECTRIC CORPORATION, Research and Development Center, 1310 Beulah Road, Pittsburgh, PA 15235

R. J. Bratton

169-170. WILLIAMS INTERNATIONAL CORPORATION, 2280 West Maple Road, Walled Lake, MI 48088

William Chapman
Peter Nagy

171. DOE, ENERGY CONVERSION & UTILIZATION TECHNOLOGIES DIVISION, Route Symbol CE-142, Forrestal Building, Washington, DC 20545

J. J. Eberhardt

172-173. DOE, MORGANTOWN ENERGY TECHNOLOGY CENTER, P.O. Box 880, Morgantown, WV 26505

D. Dubis
J. S. Wilson

174. DOE, OFFICE OF BASIC ENERGY SCIENCES, Division of Materials Sciences, ER-131, GTN, Washington, DC 20545

I. R. Thomas

175. DOE, OFFICE OF FOSSIL ENERGY, FE-14, Mail Stop B127, GTN, Washington, DC 20545

F. M. Glaser

176-177. DOE, OFFICE OF VEHICLE AND ENGINE RESEARCH AND DEVELOPMENT, Forrestal Building, 1000 Independence Avenue, Washington, DC 20585

A. A. Chesnes
R. B. Schulz

178. DOE, PITTSBURGH ENERGY TECHNOLOGY CENTER, P.O. Box 10940, Pittsburgh, PA 15236

S. W. Chun

179. DOE, OAK RIDGE OPERATIONS OFFICE, P.O. Box 2001, Oak Ridge, TN 37831

Office of Assistant Manager for Energy Research and Development

180-189. DOE, OFFICE OF SCIENTIFIC AND TECHNICAL INFORMATION, P.O. Box 62, Oak Ridge, TN 37831

For distribution by microfiche as shown in DOE/TIC-4500, Distribution Category UC-103 (Fluidized Bed Combustion), UC-105 (Flue Gas Cleanup), UC-106 (Gas Stream Cleanup), UC-108 (Coal Liquefaction), UC-109 [Coal Gasification (Surface and Underground)] UC-110 (Fuel Cells), UC-111 (Heat Engines), and UC-114 (Coal Based Materials and Components).